https://doi.org/10.5194/egusphere-2026-3923
Preprint. Discussion started: 20 July 2026

Ecosystem mobilization of subsurface water revealed by global active root-zone storage

Shijie Jiang[1,2], Georgios Blougouras[1,2,3]

[1]Department Biogeochemical Integration, Max Planck Institute for Biogeochemistry, Jena, 07745, Germany
[2]ELLIS Unit Jena, Jena, 07743, Germany
[3]Department of Geography, Friedrich Schiller University Jena, Jena, 07743, Germany

Correspondence to: Shijie Jiang (sjiang@bgc-jena.mpg.de)

Abstract. Subsurface water sustains vegetation between precipitation events and shapes ecosystem responses to hydroclimatic variability. Yet existing observations capture either near-surface soil moisture or bulk terrestrial water storage, leaving the dynamic component of subsurface water that vegetation actively mobilizes poorly understood at the global scale. Here we analyze a global reconstruction of active root zone water storage (aS_{rz}), defined as the depth of subsurface water ecosystems actively mobilize for evapotranspiration, from 2001 to 2020. The global area-weighted mean aS_{rz} is about 100 mm, with the largest values concentrated where precipitation supply and atmospheric demand are climatologically comparable. Trends in climatic water balance are most strongly reflected in aS_{rz} in seasonally driven systems such as croplands, savannas, and seasonal forests, and more weakly in evergreen tropical forests and tundra. The turnover time of the active component distinguishes rapidly cycled storage in warm and seasonally dry regions from slowly cycled storage in boreal and Arctic regions. Comparison with satellite gravimetry shows that aS_{rz} co-varies with bulk terrestrial water storage at monthly scales, but the coupling weakens and becomes more regime-dependent at interannual scales, especially in snow-dominated and dry regions. These patterns identify where bulk storage provides information on subsurface water accessed by ecosystem and where changes in bulk storage mainly reflect changes in other water stores. Overall, these findings establish ecosystem-accessed water storage as an observation-based dimension of the terrestrial water cycle, revealing patterns of ecosystem water access and change that bulk storage and climatic wetness indicators do not resolve, and providing a foundation for assessing ecosystem water vulnerability under hydroclimatic change.

1 Introduction

The ability of terrestrial ecosystems to sustain transpiration and carbon uptake during dry periods, and to moderate land surface temperature through latent heat loss, depends on how much subsurface water vegetation can continue to access after the soil surface has dried (Green et al., 2019; Humphrey et al., 2021; Seneviratne et al., 2010). This water is held in unsaturated stores, weathered substrate, and shallow groundwater connections, and is supplied by earlier rainfall, snowmelt,

https://doi.org/10.5194/egusphere-2026-3923
Preprint. Discussion started: 20 July 2026

or lateral inflow (Fan et al., 2017; McCormick et al., 2021; Rempe and Dietrich, 2018). By buffering evapotranspiration (ET) beyond individual precipitation events, the root-zone water storage shapes how vegetation activity, surface temperature, and near-surface humidity evolve during droughts, heat waves, and shifts in snowmelt timing (Gao et al., 2024). Recent multi-year droughts in the Amazon (Saatchi et al., 2013), the western United States (Goulden and Bales, 2019), and central Europe (Schuldt et al., 2020) have been associated with pronounced drawdown of subsurface water alongside vegetation dieback, multi-year reductions in carbon uptake, and amplified surface heating. The volume of this storage and the rate at which it is depleted vary substantially across landscapes and ecosystems (Gao et al., 2014; Koster and P. Mahanama, 2012), and both the volume and the depletion rate are changing as precipitation (Lesk and Mankin, 2026), snowmelt (Myers-Smith et al., 2020), and atmospheric demand shift (Qing et al., 2023) under continued warming. Quantifying how much subsurface water is present, and how much of it is accessed by vegetation, is therefore important to anticipating where ecosystems can maintain function under hydroclimatic shifts (Bachofen et al., 2024) and how vegetation water access feeds back into land-atmosphere exchange (Seneviratne et al., 2010).

Existing observational approaches to quantify this subsurface buffer differ in what they sense. Satellite microwave retrievals of surface soil moisture (e.g., Dorigo et al., 2017; Entekhabi et al., 2010) provide frequent and spatially continuous constraints on near-surface wetness and have reshaped large-scale studies of ecosystem water limitation, drought monitoring, and land-atmosphere coupling. However, the observed layer is typically only the upper few centimeters of the soil column and therefore mainly reflects recent wetting and drying. Terrestrial water storage anomalies (TWSA) from satellite gravimetry (Landerer et al., 2020) extend the view below the surface and have become central to studies of groundwater depletion (Rodell et al., 2018), ecosystem drought response (Humphrey et al., 2018), and vegetation functioning (Khanal et al., 2024). As a bulk and spatially coarse signal, however, TWSA aggregates soil water, groundwater, snow, surface water, and managed storage, each with different timing and different degrees of connection to vegetation water access. TWSA can therefore contain information on ecosystem water availability under some hydroclimatic regimes and timescales, but the fraction of the bulk signal that ecosystems actively mobilize cannot be isolated from gravimetry alone. Existing observations therefore leave the dynamic storage component accessed by ecosystems only partially resolved.

Land surface models and land data assimilation systems can estimate root-zone soil moisture directly, but their internal states depend on prescribed rooting depths, soil hydraulic properties, and plant water uptake formulations that remain weakly constrained by observations (Fisher and Koven, 2020; Warren et al., 2015). Even with data assimilation, modeled states remain tied to predefined soil layers (Reichle et al., 2019), describing where water resides in a prescribed soil column instead of how much of it is functionally exchanged with vegetation. Physical soil moisture residing within a defined root-zone layer and ecologically active water storage can therefore diverge. Part of the water in the nominal root zone is unavailable to vegetation, for example water held below the wilting point, while landscapes promoting deep-rooted vegetation or shallow-groundwater conditions may draw on water beyond the nominal root zone (Fan et al., 2017). A complementary class of

https://doi.org/10.5194/egusphere-2026-3923
Preprint. Discussion started: 20 July 2026

diagnostic approaches moves toward an observation-based functional view by inferring an apparent root-zone storage capacity from the cumulative water deficit that vegetation must bridge between recharge events (Gao et al., 2014; Stocker et al., 2023; Wang-Erlandsson et al., 2016). These methods produce biome-scale estimates of how much water vegetation needs to access to sustain observed ET. However, they target a capacity, which is an inferred bound on storage requirement at a specified return period, rather than the time-varying state that ecosystems actually mobilize. The recharge and drawdown dynamics of the storage accessed by ecosystems, and how these dynamics are shifting under hydroclimatic change, therefore fall outside this framing, even though they reveal the timing, magnitude, and persistence of ecosystem reliance on stored subsurface water.

To diagnose the ecologically active component of subsurface storage, (Blougouras et al., 2025) introduced active root zone water storage (aS_{rz}), which represents the time-varying water volume that ecosystems actively mobilize for ET, tracked relative to the lowest state observed at each grid cell over the analysis period (**Fig. 1**). Unlike volumetric root-zone soil moisture provided by conventional models, which is reported as a fraction over a prescribed modeled soil layer, aS_{rz} is reported as a depth of water, in mm, without requiring a prescribed rooting depth or soil thickness assumptions. The absolute size of this reservoir cannot be fully constrained from available observations, but the range over which it has been drawn down during the analysis period can. aS_{rz} captures this observable active range, providing a quantity that is consistent with the underlying water balance and tracked through time. As a natural extension, aS_{rz} can be directly compared with ET to yield the turnover time of the ecosystem-accessible reservoir.

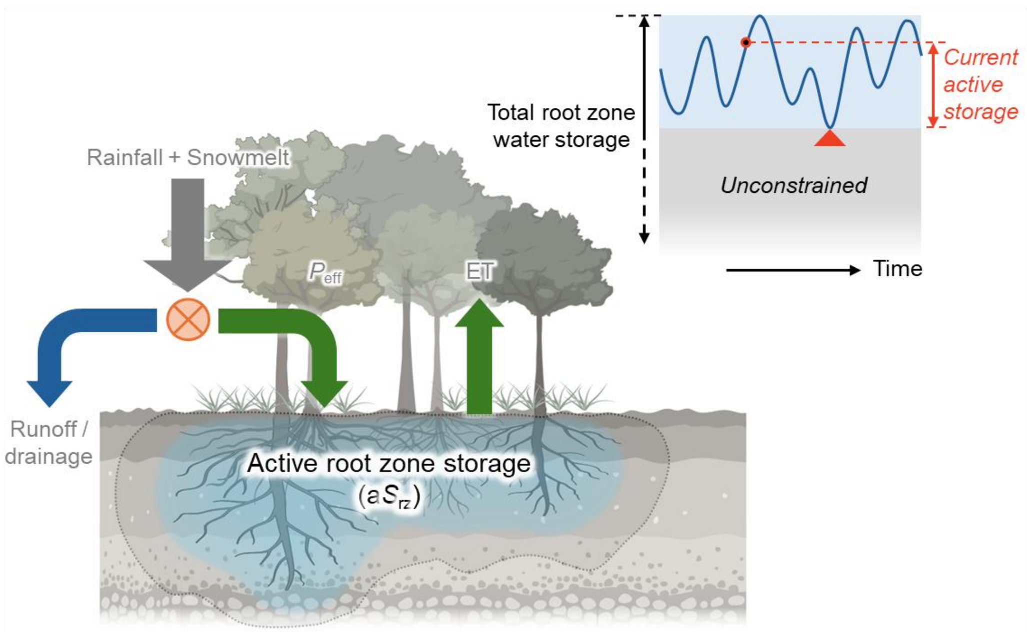

https://doi.org/10.5194/egusphere-2026-3923
Preprint. Discussion started: 20 July 2026

Figure 1. Active root zone water storage (aS_{rz}) as the ecosystem-accessible component of subsurface storage. The left diagram illustrates how aS_{rz} fits into the surface water balance. aS_{rz} is the water within an ecosystem-accessible reservoir that vegetation actively mobilizes for evapotranspiration (ET). It is recharged by effective input from rainfall and snowmelt ($\mathrm{P_{eff}}$) and depleted by ET, while water that drains to runoff or to deeper layers is separated from this reservoir. The upper right panel illustrates how aS_{rz} is defined from the modeled ecosystem-accessible storage. The full amount of subsurface water potentially connected to vegetation cannot be uniquely separated from other storage components using available observations, but the dynamic portion that ecosystems actively draw upon can be diagnosed. aS_{rz} at any moment is defined as the current state of the reservoir relative to its observed minimum over the analysis period (red triangle), capturing the active component (light blue) without requiring knowledge of the unconstrained background storage (grey).

Building on this framework, we use a global reconstruction of aS_{rz} produced with a hybrid ecohydrological framework that infers the active state from joint observations of ET, runoff, TWSA, and snow water equivalent (SWE) (Blougouras et al., 2026). The goal of this study is to quantify how subsurface storage accessed by ecosystems is organized, changing, and cycled at the global scale, and to assess when bulk terrestrial water storage carries information on this active component. We address three questions. (1) How is active root zone storage distributed globally, and how does it vary across hydroclimatic and land surface conditions? (2) Where has active storage increased or declined over recent decades, and how has the turnover of the active reservoir accelerated or slowed alongside these changes? (3) When and where does bulk terrestrial water storage provide information about active storage across seasonal and interannual timescales, and where do changes in bulk storage mainly reflect water stores not actively accessed by ecosystems? Overall, these analyses identify where ecosystem access to subsurface water is changing and where existing bulk water cycle indicators do or do not capture those changes, providing a global, observation-based basis for understanding how the terrestrial biosphere responds to hydroclimatic change.

2. Methods and Data

2.1 Active root zone water storage and its global reconstruction

We use the global aS_{rz} reconstruction developed by (Blougouras et al., 2026). The framework represents the subsurface storage accessed by ecosystems as a time-varying reservoir, S_{a}^{t}, diagnosed jointly from hydrological and ecosystem flux observations (**Fig. A1**). At each spatial unit and daily time step t, the reservoir evolves as:

$$S_{\mathrm{a}}^{t} = S_{\mathrm{a}}^{t-1} + P_{\mathrm{eff}}^{t} - \mathrm{ET}^{t} \quad (1)$$

https://doi.org/10.5194/egusphere-2026-3923
Preprint. Discussion started: 20 July 2026

where P_{eff}^{t} is the effective input from rainfall and snowmelt that enters the ecosystem-accessible reservoir. The remaining water input enters an ecosystem-inaccessible compartment that contributes to runoff and deeper drainage (**Fig. 1**). aS_{rz} is then defined as the active range of S_{a} relative to its lowest value at that location over the analysis period:

$$\mathrm{a}S_{\mathrm{rz}}^{t} = S_{\mathrm{a}}^{t} - \min_{T} S_{\mathrm{a}}^{T} \tag{2}$$

where T ranges over the analysis period, here 2001 to 2020. This definition means that aS_{rz} quantifies the observed dynamic range of subsurface storage accessed by ecosystems, not the absolute amount of water stored belowground. Although the reference minimum is necessarily tied to the climatic conditions sampled within a finite record, sensitivity tests using progressively expanding windows from 1 to 20 years show that climatological mean aS_{rz} stabilizes as the window approaches 20 years across major vegetation classes (**Fig. S1** in the Supplement). The 20-year baseline therefore captures the realized active storage range under the prevailing hydroclimate. The implications of this baseline choice for the magnitude and spatial robustness of aS_{rz} are discussed further in **Sect. 4**.

The reconstruction addresses the fact that neither P_{eff} nor the parameters controlling aS_{rz} dynamics are directly observed. In the underlying framework, these unknown process parameters are represented as functions of static catchment attributes, including climate, vegetation, soil, and topography, using neural networks embedded in a differentiable water-balance model. The model is trained at catchment scale against multiple observational constraints, so that simulated ET, runoff, snow water equivalent, and TWSA are matched simultaneously. The governing equations and main process parameters used to obtain aS_{rz} are summarized in **Appendix A**, while full model architecture, training objectives, sensitivity tests, and product-level evaluation are provided by (Blougouras et al., 2026).

The global reconstruction is produced at 0.25° spatial resolution for 2001 to 2020. The training uses 1,186 global catchments from the GRDC-Caravan dataset (Färber et al., 2025), restricted to drainage areas between 100 and 2,500 km^2 and to catchments with limited urban cover, irrigation, and upstream reservoir storage. Daily meteorological forcing, including precipitation, temperature, and net radiation, is obtained from ERA5-Land (Muñoz-Sabater et al., 2021), and daily leaf area index (LAI) is interpolated from GIMMS LAI4g (Cao et al., 2023). Static attributes describing aridity, snow cover, terrain, soil texture, and land cover fractions are taken from HydroATLAS (Linke et al., 2019) and SoilGrids (Poggio et al., 2021). The observational targets are taken from FLUXCOM X-BASE (Nelson et al., 2024) for ET, GRDC-Caravan for runoff, ERA5-Land for snow water equivalent, and GRACE(-FO) mascon products (Watkins et al., 2015) for TWSA. Each target contributes equally to the training loss through its Nash-Sutcliffe efficiency.

Uncertainty related to catchment sampling and neural-network initialization is represented using five-fold spatial cross-validation combined with five random seeds, yielding 25 model instances. Each instance is applied independently to the global grid using gridded forcing and static attributes from the same data sources, and the ensemble mean is aggregated from daily to monthly time series for all subsequent analyses. We use this ensemble mean reconstruction as an observation-

https://doi.org/10.5194/egusphere-2026-3923
Preprint. Discussion started: 20 July 2026

constrained estimate of the active storage range accessed by ecosystems. Because aS_{rz} is a latent diagnostic derived from the dynamic range of S_a, it has no direct one-to-one observational counterpart. However, comparisons with independent gridded root-zone soil moisture products show that the reconstructed storage dynamics are broadly consistent with existing estimates of root-zone wetness across most vegetated land areas (**Fig. A2**).

2.2 Turnover time of the active reservoir

The size of the active reservoir alone does not determine the pace at which water cycles through it (Qing et al., 2023), because the same storage amount can imply different cycling rates depending on ET. Conversely, similar ET rates can correspond to different depletion times when the active storage differs. To characterize this pace and to track how it changes alongside aS_{rz}, we define the turnover time τ of the active reservoir as the ratio of climatological mean aS_{rz} to climatological mean ET over 2001 to 2020:

$$\tau = \frac{\overline{\mathrm{a}S_{rz}}}{\overline{\mathrm{ET}}} \tag{3}$$

Here, τ has units of days and represents the characteristic timescale over which the active reservoir would be depleted at the current rate of ET if water inputs ceased. A long τ indicates slow cycling of the active store relative to ET, while a short τ indicates rapid cycling and a shorter depletion timescale under interrupted water inputs. Because aS_{rz} represents the part of subsurface storage mobilized for ET within the analysis period, τ characterizes the bulk pace at which this active component is cycled through the land-atmosphere interface. Unlike transit time distributions derived from tracer data, τ does not resolve age distributions of individual water parcels, but instead measures a storage-to-outflow timescale for the active reservoir (Sprenger et al., 2019). To track changes in τ, we additionally compute annual turnover time at each grid cell as the ratio of annual mean of aS_{rz} to annual mean ET in each year from 2001 to 2020 and estimate trends in annual τ (as described in **Sect. 2.4**). For this calculation, ET is taken from FLUXCOM X-BASE (Nelson et al., 2024), aggregated to the same 0.25° grid and timescale as aS_{rz}.

2.3 Coupling between aS_{rz} and bulk terrestrial water storage

To diagnose when bulk terrestrial water storage contains information on storage accessed by ecosystems, we compare aS_{rz} with TWSA over 2003 to 2020, the overlap between the GRACE record and the aS_{rz} reconstruction. TWSA is regridded to 0.25° to match the aS_{rz} reconstruction, and both signals are compared at monthly and annual scales. At each grid cell, we compute two Pearson correlations between the paired time series. The monthly correlation uses the full monthly series and reflects joint variability across all timescales captured by both signals, although it is in practice dominated by the shared seasonal cycle in many regions. The interannual correlation uses annual means and isolates year-to-year coupling after seasonal variability has been averaged out. Because TWSA aggregates soil water, groundwater, snow, surface water, and managed store, while aS_{rz} represents the ecosystem-accessible component of subsurface storage, comparing the two

https://doi.org/10.5194/egusphere-2026-3923
Preprint. Discussion started: 20 July 2026

correlations diagnoses where and at which timescales the active reservoir and the bulk storage signal evolve together. Grid cells with multi-year mean snow cover fraction above 75% are flagged in subsequent analyses, because the TWSA signal in these regions is strongly affected by SWE and is unlikely to track the same processes as aS_{rz} (Frappart et al., 2006). Snow cover fraction is taken from HydroATLAS (Linke et al., 2019), which aggregates MODIS daily snow cover (MYD10A1) into a multi-year mean snow extent, here resampled to 0.25°.

2.4 Spatial and temporal analyses

All analyses use monthly aS_{rz} time series obtained by aggregating the daily reconstruction over 2001 to 2020. The analysis domain covers all land grid cells with an assigned vegetation class based on the MODIS modified IGBP classification (Friedl et al., 2010), originally available at 30 arc-second resolution and aggregated to 0.25° by retaining the dominant vegetation type within each grid cell (**Fig. S2** in the Supplement); Greenland and Antarctica are excluded. We compute annual precipitation P from ERA5-Land, consistent with the forcing used to produce aS_{rz}, and annual potential evapotranspiration (PET) independently using the Priestley-Taylor formulation (Priestley and Taylor, 1972) with $\alpha = 1.26$ and net radiation, air temperature, and surface pressure from ERA5-Land. The resulting climatological P, PET, and aridity index P/PET fields are shown in **Fig. S3** in the Supplement. Temporal trends are computed at each grid cell using the Mann-Kendall test combined with the Theil-Sen slope estimator on annual series from 2001 to 2020. We compute trends for annual aS_{rz}, annual τ, and annual climatic water balance (P−PET). For each land cover type, we quantify the sensitivity β of aS_{rz} trends to climatic water balance trends as the slope of an ordinary least squares regression of grid-cell aS_{rz} trends against grid-cell climatic water balance trends within that land cover class. Confidence intervals for β are estimated using 1,000 bootstrap replicates.

3 Results and Discussions

3.1 Climatology and controls of active root zone water storage

The reconstructed climatology of aS_{rz} over 2001 to 2020 has a global area-weighted mean of 97 mm, excluding Greenland and Antarctica, and shows large spatial variability, from values near zero across the driest regions to values exceeding 300 mm in parts of the wet tropics and subtropics (**Fig. 2a**). Time series at four representative grid cells illustrate how the active storage range differs across different ecosystems and aridity conditions (**Fig. 2b-e**). In a continuously humid Amazon evergreen broadleaf forest, aS_{rz} is relatively moderate, with a mean of 84 mm, despite the wet subsurface conditions indicated by the large modeled ecosystem-accessible storage S_a (**Fig. 2b**). This is consistent with shallow and continuously available water supply that limits the range over which storage must be drawn down (Miguez-Macho and Fan, 2012). In a southeastern deciduous broadleaf forest in the United States, aS_{rz} exceeds 200 mm and varies strongly through the seasonal cycle (**Fig. 2c**). In a semi-arid savanna, aS_{rz} swings between near-zero and around 400 mm each year, with a mean 192 mm (**Fig. 2d**). In an East Asian grassland, aS_{rz} remains small, with a mean of 37 mm and a narrow active storage range (**Fig. 2e**).

https://doi.org/10.5194/egusphere-2026-3923
Preprint. Discussion started: 20 July 2026

200 Notably, the deciduous broadleaf forest and the grassland have nearly identical aridity index value (AI = 1.05), yet differ in mean aS_{rz} by nearly a factor of six. Therefore, aridity alone does not determine how much subsurface water is mobilized; vegetation structure and ecosystem water use strategy also strongly shape the active storage range (Fan et al., 2017; Gao et al., 2024; Schenk and Jackson, 2002).

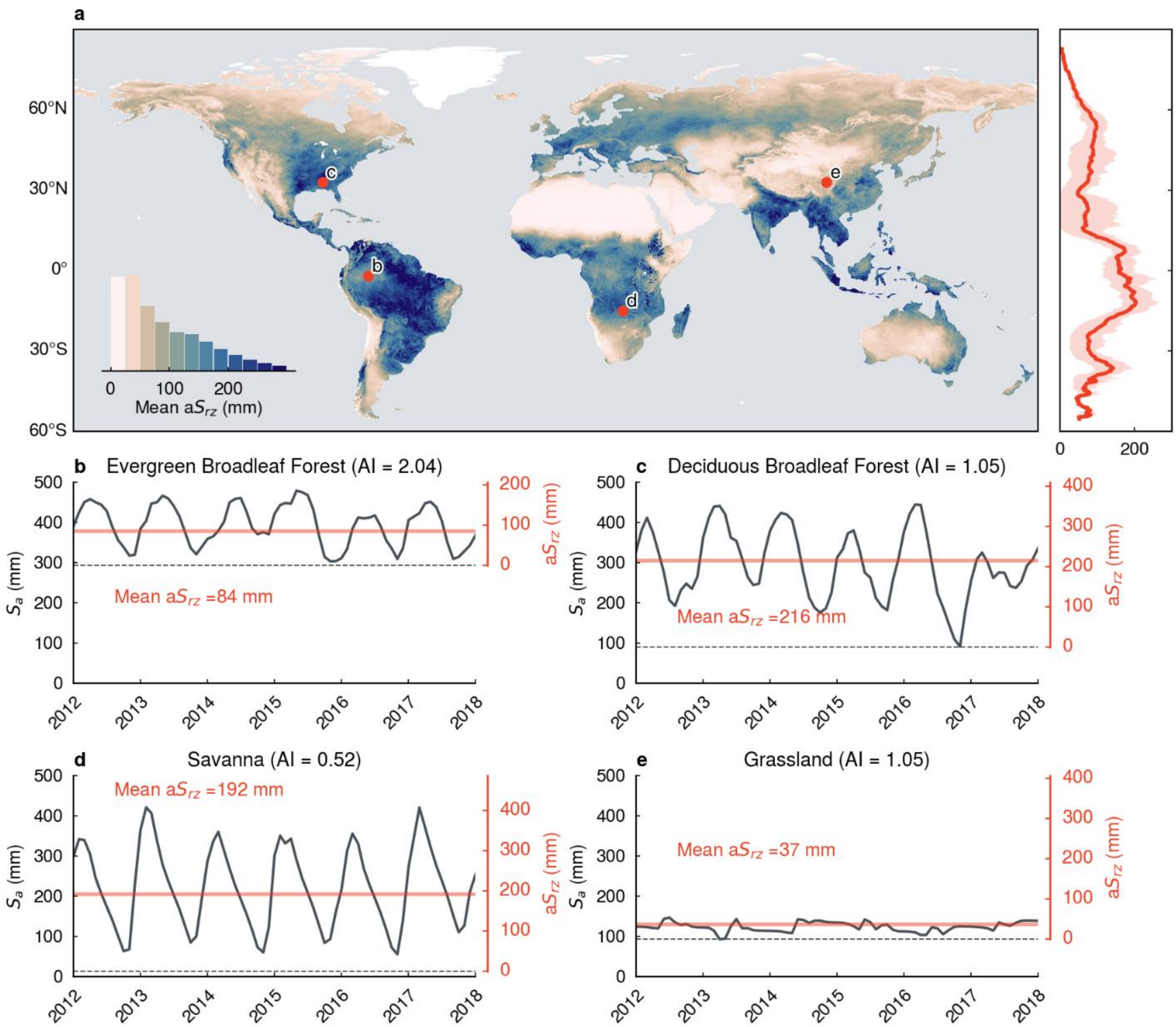

205 **Figure 2. Global distribution of mean active root zone water storage (aS_{rz}) and representative time series.** (a) Climatological mean aS_{rz} over 2001 to 2020. The inset histogram shows the global distribution of grid-cell mean aS_{rz}. The right panel shows the zonal mean, with shading indicating with the 25th to 75th percentile range. Red dots labelled b-e mark

https://doi.org/10.5194/egusphere-2026-3923
Preprint. Discussion started: 20 July 2026

four grid cells whose time series are shown in panels b to e. (**b-e**) Monthly time series of modeled ecosystem-accessible water storage S_a on the left axis and the corresponding active component aS_{rz} on the right axis over 2012 to 2018 at four representative grid cells: (**b**) Amazon evergreen broadleaf forest, (**c**) southeastern US deciduous broadleaf forest, (**d**) southern African savanna, and (**e**) northern China grassland. AI denotes the aridity index, defined as P/PET.

These patterns are consistent with earlier estimates of root-zone storage capacity based on climatic water deficits, which show low values in continuously wet tropical forests, larger values where seasonal water limitation favors deeper storage access, and reduced values in grasslands that often respond to drought through dormancy instead of deep water uptake. (Knapp et al., 2008; Stocker et al., 2023; Wang-Erlandsson et al., 2016). In the analysis below, we focus on aS_{rz} instead of S_a, which is shown in Fig. 2 only to illustrate how this active range is defined relative to the modeled storage trajectory; aS_{rz} captures the observed active range of ecosystem-accessible storage during the analysis period.

The non-monotonic dependence of mean aS_{rz} on climate is also evident globally (**Fig. 3a**). Across the global P and PET space, mean aS_{rz} peaks where annual precipitation is comparable to annual PET and decreases toward both arid and very humid extremes (Gao et al., 2014). As shown in the inset of **Fig. 3a**, median aS_{rz} rises from below 50 mm in arid conditions to above 100 mm in dry sub-humid and humid conditions, then declines again in very humid regions. The largest active reservoirs therefore occur not at the wet end of the moisture gradient, but where seasonal mismatch between supply and atmospheric demand requires sustained reliance on stored water to maintain ET. Within each climatic class, vegetation activity further structures the active storage magnitude (**Fig. 3b**). The dependence on mean LAI is strongest from semi-arid to humid climates, where median aS_{rz} increases from around 30 mm at LAI < 0.5 to above 200 mm at LAI > 3.0. In very humid climates, the LAI gradient remains visible but weakens at high LAI, consistent with the Amazon example in **Fig. 2b**, where dense vegetation does not require a large active drawdown range under continuously wet conditions. Soil texture and topography add further controls within the same climatic condition. Mean aS_{rz} is larger on gentle terrain than on steep slopes (**Fig. 3c**), consistent with deeper soil development and more sustained water retention on low-relief landscapes, whereas steep terrain favors shallow soils and faster drainage (Fan et al., 2017; Gnann et al., 2025). Sand fraction shows a broadly negative relationship with aS_{rz} (**Fig. 3d**), consistent with the low water-holding capacity of coarse-textured soils and their limited retention against gravity (Fatichi et al., 2020; Wankmüller et al., 2024).

https://doi.org/10.5194/egusphere-2026-3923
Preprint. Discussion started: 20 July 2026

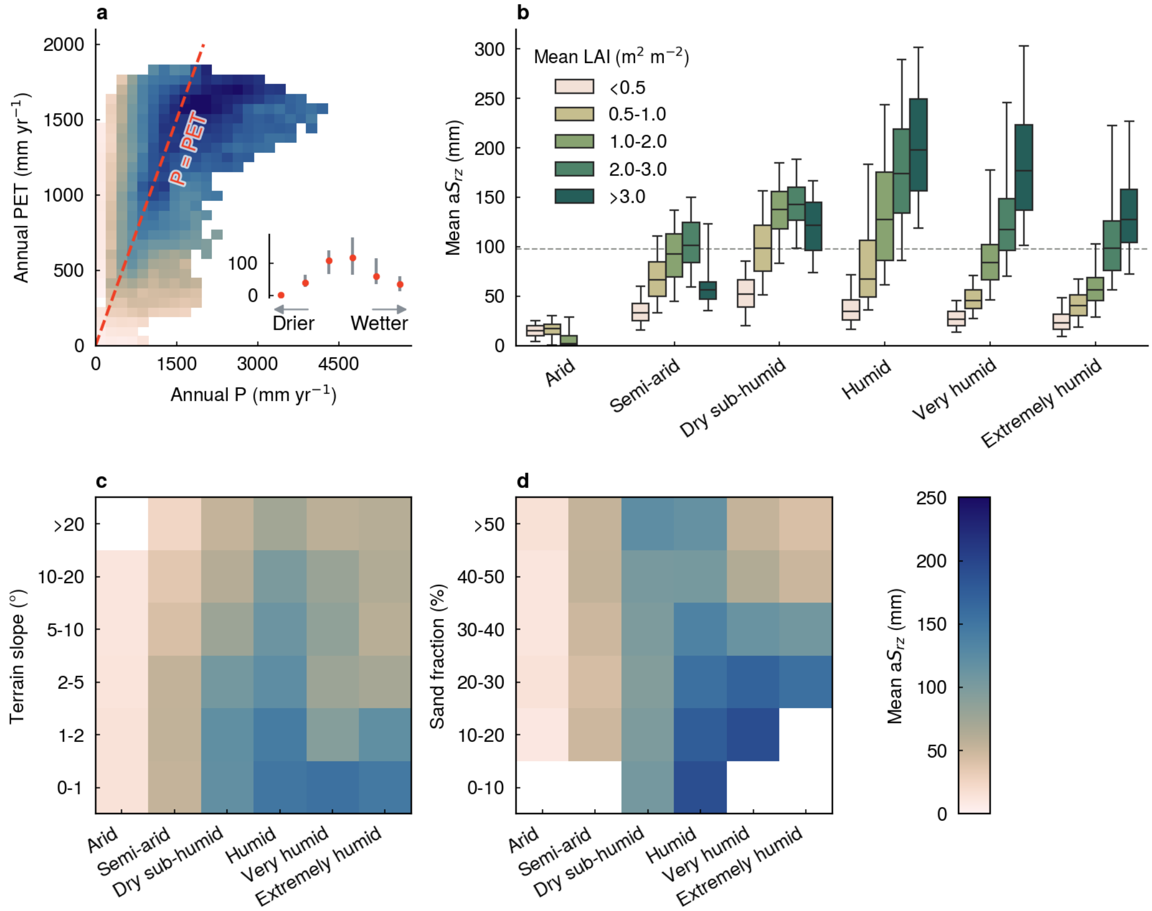

Figure 3. Mean aS_{rz} across climate, vegetation, terrain, and soil. (**a**) Mean aS_{rz} across the global precipitation (P) and potential evapotranspiration (PET) space. Each bin shows the mean aS_{rz} over all grid cells with the corresponding annual P and annual PET. Bins with fewer than 25 valid grid cells are masked. The red dashed line marks P=PET. The inset shows the median and 25th to 75th percentile range of mean aS_{rz} across aridity classes ordered from drier to wetter. (**b**) Mean aS_{rz} stratified by aridity class and mean leaf area index (LAI). Aridity classes are defined by P/PET: arid < 0.20, semi-arid 0.20-0.50, dry sub-humid 0.50-0.65, humid 0.65-1.5, very humid 1.5-3.0, and extremely humid > 3.0. Boxes show the 25th to 75th percentiles, whiskers extend to 1.5 times the interquartile range, and the horizontal dashed line marks the global area-weighted mean. (**c**) Mean aS_{rz} stratified by aridity class and terrain slope. (**d**) Mean aS_{rz} stratified by aridity class and sand fraction of the soil. In panels c and d, each cell shows the mean aS_{rz} over all grid cells with the corresponding combination of aridity class and physical attribute; white cells indicate combinations with fewer than 25 valid grid cells.

https://doi.org/10.5194/egusphere-2026-3923
Preprint. Discussion started: 20 July 2026

3.2 Recent changes in active storage and reservoir turnover

The active reservoir does not show a globally dominant trend direction over 2001–2020 (**Fig. 4a**). Area-weighted fractions of grid cells with positive and negative trends are nearly balanced, 50.4% and 49.6%, respectively, and about 6% of grid cells show trends significant at $p<0.05$, split similarly between the two directions. This relatively small fraction of significant local trends is expected for a 20-year annual record, where interannual variability reduces the power to detect monotonic changes at individual grid cells. Nevertheless, the trend field shows coherent regional structure. Western and eastern Europe, parts of east Asia, southern Africa, and the southern and eastern margins of the Amazon show declining aS_{rz}, while the Sahel, parts of the Indian subcontinent, the southeastern United States, the maritime continent, and eastern Australia shows increasing aS_{rz}. The broad geography of these trends overlaps with reported TWSA changes in some regions, including declines in Europe and Brazil (Lu et al., 2025), but diverges in others, such as the southeastern United States, where total storage trends may be strongly affected by groundwater changes that are not directly tied to ecosystem water access. This divergence motivates the explicit comparison with TWSA in **Sect. 3.3**.

https://doi.org/10.5194/egusphere-2026-3923
Preprint. Discussion started: 20 July 2026

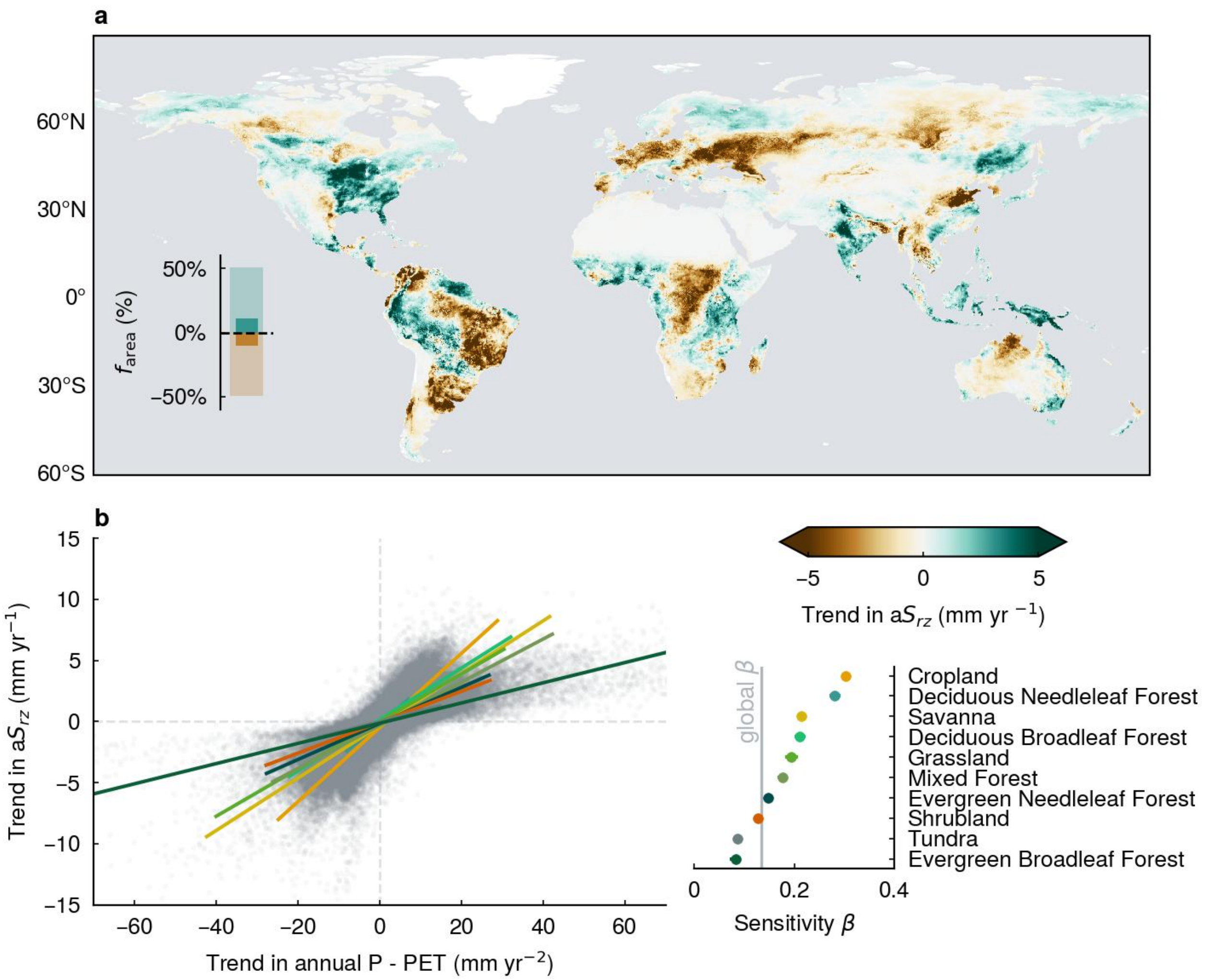

Figure 4. Recent trends in active root zone water storage and their sensitivity to climatic water balance. (**a**) Trend in annual aS_{rz} over 2001 to 2020 at each grid cell. The inset bar chart shows the area fraction of grid cells with positive and negative trends, with darker shading indicating trends significant at $p < 0.05$. (**b**) Relationship between trends in annual aS_{rz} and annual P−PET across grid cells. Grey points show individual grid cells, and colored lines show ordinary least squares regressions fitted separately for each land cover type. The right panel shows the sensitivity β of aS_{rz} trends to P−PET trends for each land cover type, estimated as the corresponding regression slope. Horizontal bars show 99% confidence intervals estimated by bootstrapping. The vertical dashed line marks the global β across all grid cells.

https://doi.org/10.5194/egusphere-2026-3923
Preprint. Discussion started: 20 July 2026

Trends in aS_{rz} broadly follow trends in climatic water balance, defined here as P−PET (**Fig. 4b** and **Fig. S4** in the Supplement). Regions shifting toward drier climatic water balance tend to be losing active storage, whereas regions shifting toward wetter balance tend to gain active storage. However, changes in climatic water balance are not expressed uniformly across ecosystems. Croplands, deciduous needleleaf forests, savannas, deciduous broadleaf forests, and grasslands show the steepest sensitivities, reaching about twice the global mean sensitivity, β = 0.13 mm per mm of P−PET. These ecosystems share pronounced seasonal cycles of water use, during which the active reservoir is filled and drawn down through a wide dynamic range. As a result, shifts in climatic water balance are more strongly reflected in aS_{rz}. In contrast, evergreen broadleaf forests and tundra show sensitivities close to half the global mean. In evergreen broadleaf forests, water is rarely the primary constraint on ET, so vegetation activity and active storage respond more weakly to changes in climatic water balance (Restrepo-Coupe et al., 2013). In tundra, water use is also constrained by temperature and growing-season length (Myers-Smith et al., 2020). These results indicate that hydroclimatic change is more strongly expressed in active storage within seasonally driven ecosystems, including the major croplands, savannas, and seasonal forests, where changes in subsurface water access are most relevant for vegetation productivity, carbon uptake, and drought response (Lesk et al., 2016; Vicente-Serrano et al., 2013).

To characterize how rapidly the active reservoir cycles, we examine the turnover time τ, defined as the ratio of mean aS_{rz} to mean ET. Mean τ varies by more than an order of magnitude across the land surface (**Fig. 5a**). The longest values, exceeding 150 days, occur across boreal and Arctic regions, where low ET leads to slow cycling of the active reservoir. Values of 50 to 100 days are typical of temperate forests and croplands, while τ shorter than 50 days is common across the wet tropics, seasonally dry savannas, and semi-arid grasslands and shrublands. In these regions, high ET produces rapid cycling even where active storage is large in absolute terms (**Fig. 5b**). Trends in annual τ over 2001 to 2020 show where the pace of the active water cycle has changed (**Fig. 5c**). Shortening τ, indicating faster turnover, occurs across much of Europe, western North America, parts of central Asia, southern Africa, and the southeastern Amazon. Lengthening τ, indicating slower turnover, occurs across Alaska, northern Canada, the Sahel, the Indian subcontinent, and the southeastern United States. These patterns reflect the combined effects of trends in aS_{rz} and ET (**Fig. 4** and **Fig. S5** in the Supplement). Where declining aS_{rz} and shortening τ occur together, the active reservoir is becoming both smaller and faster to cycle through. In ecosystems with strong seasonal water use and limited dry season recharge, this combination may reduce the duration over which subsurface storage can buffer ET and carbon uptake during dry periods (Reichstein et al., 2013), warranting further analysis with independent vegetation and flux observations.

https://doi.org/10.5194/egusphere-2026-3923
Preprint. Discussion started: 20 July 2026

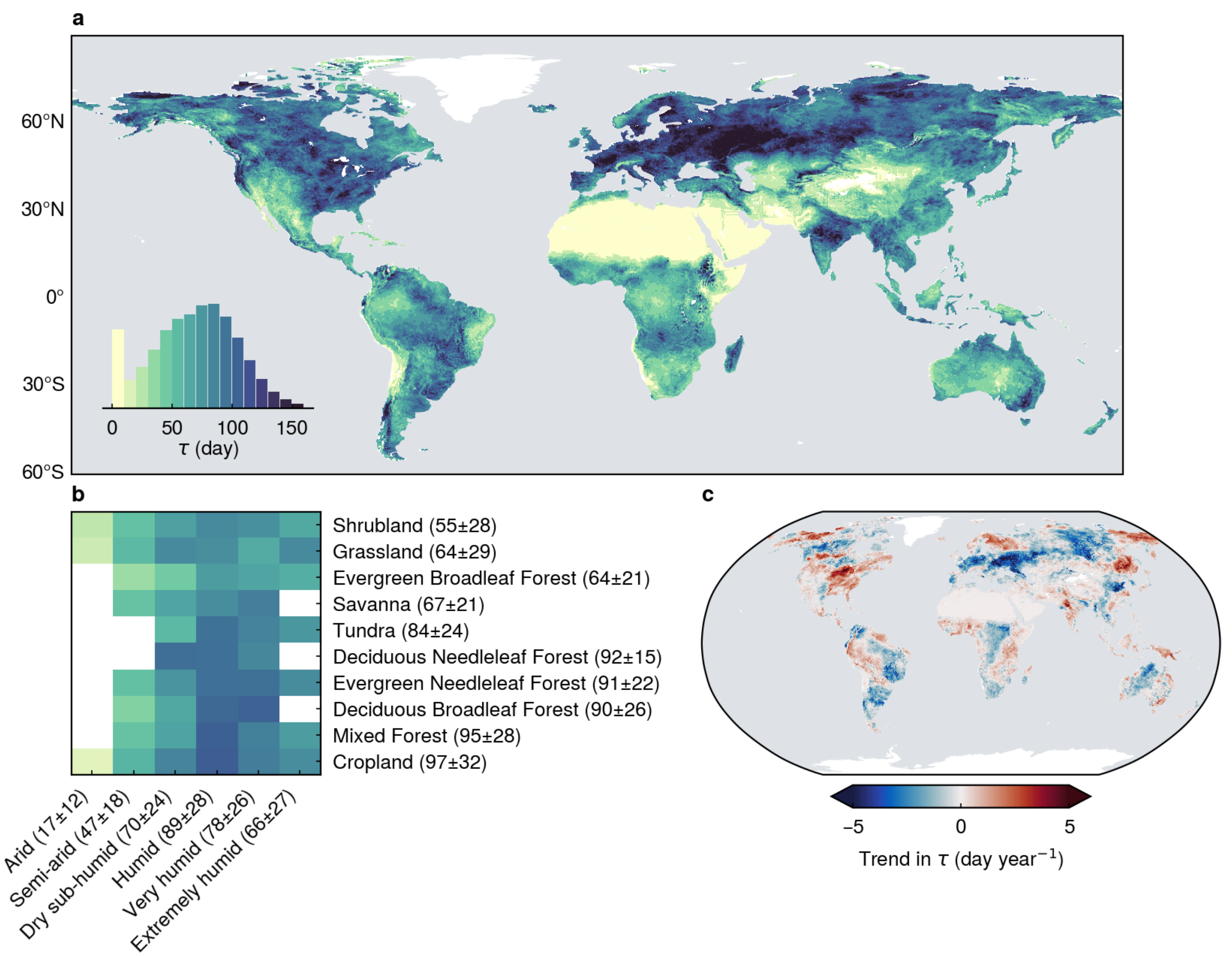

295 **Figure 5. Turnover time of the active reservoir.** (**a**) Climatological mean turnover time τ, defined as the ratio of mean aS_{rz} to mean ET over 2001 to 2020, at each grid cell. The inset histogram shows the global distribution of grid-cell mean τ. (**b**) Mean τ stratified by land cover type, rows, sorted by median τ, and aridity class, columns. Aridity classes are defined by P/PET: arid < 0.20, semi-arid 0.20-0.50, dry sub-humid 0.50-0.65, humid 0.65-1.5, very humid 1.5-3.0, extremely humid > 3.0). Values in parentheses give the mean τ and standard deviation in days for each land cover type and aridity class. Only
300 combinations with more than 25 valid grid cells are shown. (c) Trend in annual τ over 2001 to 2020 at each grid cell. Blue indicates faster turnover (shortening τ) and red indicates slower turnover (lengthening τ).

https://doi.org/10.5194/egusphere-2026-3923
Preprint. Discussion started: 20 July 2026

3.3 Decoupling between active storage and bulk terrestrial water storage

TWSA from satellite gravimetry is increasingly used as a proxy for root-zone water availability in ecosystem studies (Gentine et al., 2019; Humphrey et al., 2018; Khanal et al., 2024), because it extends below the shallow layer sensed by surface soil moisture and provides global coverage where direct root-zone observations are unavailable. However, TWSA aggregates soil water, groundwater, snow, surface water, and managed storage, each with different timing and different degrees of connection to vegetation water access. The aS_{rz} reconstruction provides a functional estimate of the storage component actively accessed by ecosystems, allowing us to diagnose where and over which timescales TWSA and active root zone storage remain coupled and where they decouple. **Fig. 6a** shows the Pearson correlations at each grid cell between monthly aS_{rz} and monthly TWSA, and between their annual means. The monthly correlation reflects joint variability dominated by the seasonal cycle, whereas the interannual correlation isolates year-to-year coupling after seasonal variability has been averaged out. Across much of the land surface, aS_{rz} and TWSA co-vary strongly under shared seasonal climate forcing. Grid cells with both monthly and interannual correlations exceeding 0.6 cover roughly 70% of the analyzed land area, and the highest coupling class alone accounts for about one third of the analyzed land (**Fig. 6a** inset).

https://doi.org/10.5194/egusphere-2026-3923
Preprint. Discussion started: 20 July 2026

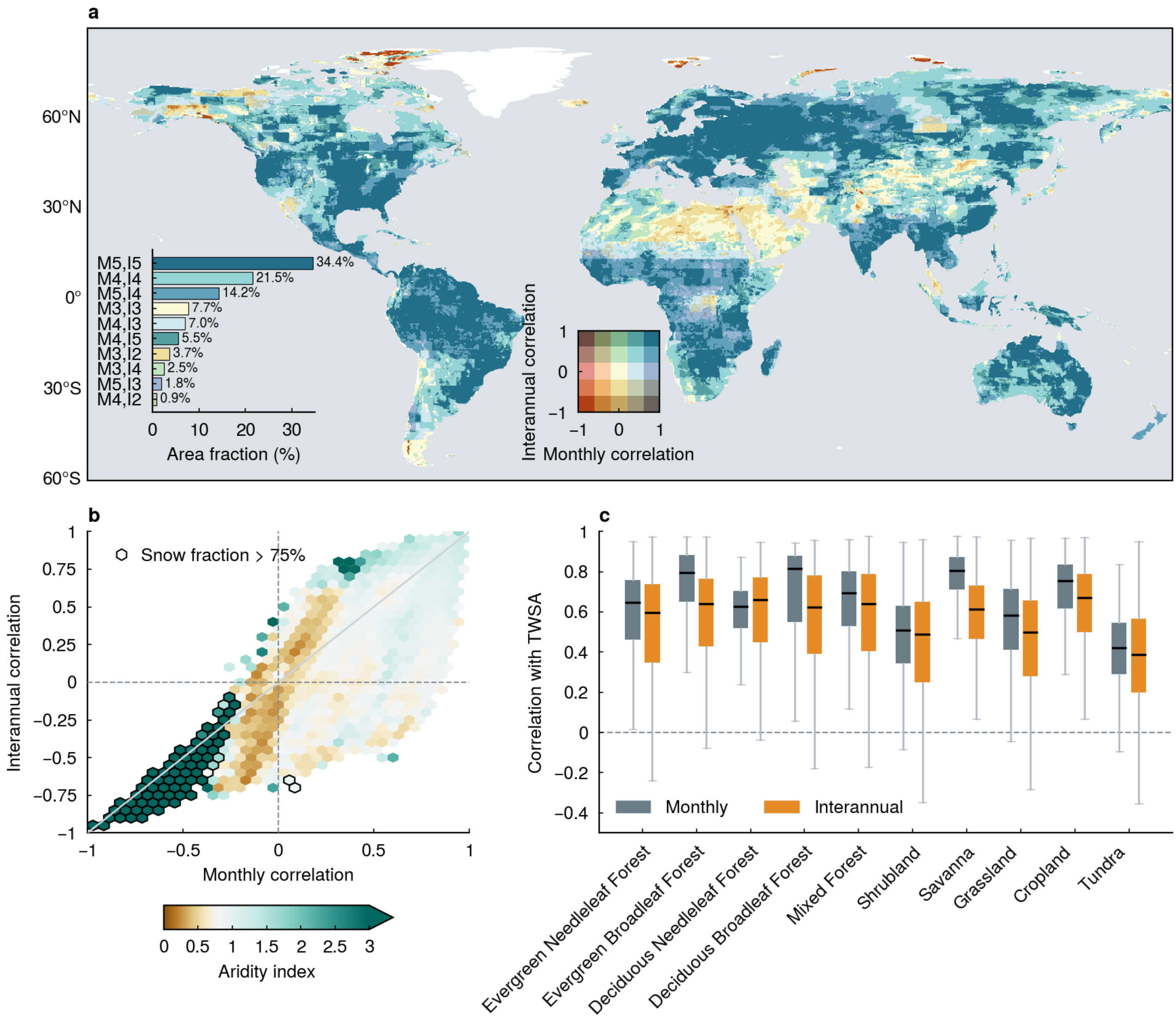

Figure 6. Coupling and decoupling between active root zone water storage (aS_{rz}) and terrestrial water storage anomalies (TWSA) across timescales, 2003–2020. (a) Bivariate map of grid-cell Pearson correlations between aS_{rz} and TWSA at monthly (M) and interannual (I) timescales. Each axis of the bivariate color legend (inset, right) is divided into five bins with edges at −1, −0.6, −0.2, 0.2, 0.6, and 1, yielding 25 categories of joint coupling strength. The bar chart (inset, left) shows the ten most extensive categories and the fraction of analyzed land area they cover. Class labels indicate monthly and interannual bins, respectively. (b) Joint distribution of monthly and interannual correlations across all analyzed grid cells, colored by aridity index, defined as P/PET. Grid cells with multi-year mean snow cover fraction above 75% are outlined. (c)

https://doi.org/10.5194/egusphere-2026-3923
Preprint. Discussion started: 20 July 2026

Distribution of monthly and interannual correlations stratified by IGBP land cover class. Boxes show the 25th to 75th percentiles, horizontal lines mark the median, and whiskers extend to 1.5 times the interquartile range.

Humid regions generally show positive correlations at both monthly and interannual timescales (**Fig. 6b**), except where snow dominates the TWSA signal (Frappart et al., 2006). In these snow-dominated grid cells, correlations are close to zero or negative because snow storage and aS_{rz} follow opposite seasonal phases. Snow accumulates when aS_{rz} is near its winter minimum and melts when the active reservoir is being replenished. The same behavior is evident for tundra in the land-cover comparison (**Fig. 6c**). In most other vegetated regions, monthly correlations are high; savannas, broadleaf forests, and croplands show especially strong monthly coupling, with median correlations around or above 0.75, indicating pronounced seasonal recharge and depletion cycles that make aS_{rz} and TWSA vary in phase with seasonal climate forcing. The annual correlations are lower and more variable, meaning that the shared seasonal cycle accounts for much of the apparent agreement between aS_{rz} and TWSA, while year-to-year variations are more strongly affected by other storage components, including groundwater, river and floodplain storage, and other water stores that are not directly tied to ecosystem water access (Humphrey et al., 2023; Scanlon et al., 2018). It is worth highlighting that savannas, where soil water availability is identified as the dominant mediator of precipitation variability on carbon fluxes, show the largest discrepancy between monthly and interannual correlations (Nadolski et al., 2026).

In arid and semi-arid regions, monthly correlations are systematically low (**Fig. 6a, b**). aS_{rz} is small in absolute magnitude in these regions, so its contribution to the bulk TWSA signal is limited, and monthly TWSA variability is shaped more by other storage components than by ecosystem-accessible storage. Interannual correlations, in contrast, vary widely across these regions. Some areas, such as interior Australia, parts of central Asia, and the Sahel margin, show moderate to high coupling, while hyper-arid regions such as the central Sahara, the Arabian Peninsula, and the Atacama show correlations near zero or strongly negative. The mechanisms governing this interannual heterogeneity are likely diverse, involving long-term groundwater trends, sporadic recharge and flood events, and large-scale climate modes (Phillips et al., 2012; Rodell et al., 2018; Werth et al., 2017).

3.4 Limitations and outlook

Although the reconstruction of aS_{rz} provides a globally consistent, observation-constrained view of subsurface storage accessed by ecosystems, several limitations should be considered when interpreting the results and point to directions for further development.

First, aS_{rz} is referenced to the observed minimum at each grid cell over 2001 to 2020. Its magnitude therefore depends on the hydroclimatic conditions sampled during this period; where the record does not include a pronounced dry-down, the reference minimum may be elevated and the active reservoir may be correspondingly underestimated. Nevertheless, a sub-

https://doi.org/10.5194/egusphere-2026-3923
Preprint. Discussion started: 20 July 2026

window analysis (**Fig. S1** in the Supplement) shows that climatological mean aS_{rz} stabilizes as the window length approaches 20 years across all major vegetation classes, with slower convergence in deciduous broadleaf forests, croplands, and savannas. In these systems, the estimated active storage is more sensitive to whether the analysis window captures years with strong seasonal drawdown or unusually severe dry conditions. The broad relative ordering of mean aS_{rz} across vegetation classes and the global spatial pattern remain consistent across window choices (**Figs. S1** and **S6** in the Supplement), indicating that the biome-level and spatial conclusions of this study are robust to the analysis period, even if absolute magnitudes in some seasonally driven systems may be modestly underestimated. Because the framework is prognostic, it can in principle be extended to longer meteorological forcing records to sample a wider range of hydroclimatic conditions, although the degree of observational constraint will vary with the availability of ET, runoff, snow, and TWSA data. Such extensions would reduce dependence on the specific drought history of 2001 to 2020, and improve estimates of the realized active storage range. Extreme value approaches based on the return period of cumulative water deficit (Stocker et al., 2023; Wang-Erlandsson et al., 2016) provide a complementary route by estimating storage requirements associated with rarer droughts than those directly observed. Combining such estimates with observation-constrained aS_{rz} could help connect what ecosystems have mobilized during the observational record with what they may need to mobilize under more extreme events.

Second, aS_{rz} is diagnosed as a latent state jointly constrained by ET, runoff, SWE, and TWSA. A key strength of the framework is that runoff provides an integrated catchment-scale water-balance constraint, which greatly broadens the observational basis beyond locations with direct vegetation or flux measurements (Jung et al., 2020; Schimel et al., 2015). It helps identify the partitioning between water retained in the ecosystem-accessible bucket and water routed to runoff and deeper drainage. However, the strength of the constraint still varies geographically because river gauges are unevenly distributed (Krabbenhoft et al., 2022). As a result, uncertainty may remain larger in regions that are weakly represented by the gauge network or where local water management, permafrost, wetlands, or tropical forest hydrology are not fully captured by the training data. Unlike streamflow or near-surface soil moisture, aS_{rz} does not have a direct one-to-one observational counterpart that can be used for straightforward validation. Its evaluation therefore relies on functional consistency across multiple lines of evidence. Future tests should examine whether aS_{rz} behaves as expected in ecologically meaningful situations, such as buffering ET during meteorological drought (Miralles et al., 2019), sustaining canopy activity through dry-down periods (Noormets et al., 2008), or recovering after extreme dry years (Schwalm et al., 2017), and whether these behaviors agree with independent vegetation, flux, and remotely sensed stress indicators.

Third, aS_{rz} quantifies the net storage range that ecosystems actively mobilize for ET, but it does not resolve the source pathways that supply this water. The active reservoir may be fed by shallow unsaturated stores, deeper weathered substrate, or shallow groundwater connections (McCormick et al., 2021; Rempe and Dietrich, 2018). At a given location, it may also be affected by lateral subsurface flow from upslope areas (Fan et al., 2019; Maxwell and Condon, 2016), hydraulic redistribution within root systems (Neumann and Cardon, 2012), or riparian and floodplain exchanges with surface water

(Yang et al., 2025). These contributions can vary substantially across landscapes and may decouple aS_{rz} from the local vertical water balance, particularly in regions with strong topographic gradients, shallow water tables, or floodplain connectivity. Disentangling these source pathways is beyond the scope of the present analysis but is important for linking active storage dynamics to subsurface hydrological processes and for understanding how ecosystems sustain water access under variable supply.

4 Conclusions

In this study, we used a global, observation-constrained reconstruction of active root-zone water storage to analyze how subsurface storage accessed by ecosystems is distributed, changing, cycled, and reflected in bulk terrestrial water storage. The results show that aS_{rz} behaves as a distinct component of the terrestrial water cycle whose magnitude and dynamics are jointly governed by climatic supply, atmospheric demand, and how ecosystems mobilize and use that supply. Its largest values occur not where water is most abundant, but where supply and demand are comparable, because the reservoir reflects the water vegetation routinely draws upon instead of the amount of water that is meteorologically available. Within each climatic regime, vegetation activity, soil texture, and terrain further regulate active storage behavior (**Figs. 2** and **3**). Recent changes in aS_{rz} show no globally dominant trend direction over 2001 to 2020, but they reveal coherent regional increases and declines. In particular, trends in climatic water balance are expressed most strongly in seasonally driven systems that fill and empty the active reservoir each year, and more weakly in systems where water is rarely limiting or where energy and growing-season length also constrain water use (**Fig. 4**). These storage changes are accompanied by changes in reservoir turnover, showing that the active water cycle's size and pace are both changing (**Fig. 5**). This regime dependence can be also found in the relationship with bulk terrestrial water storage (**Fig. 6**). The result suggests that TWSA can provide useful information on ecosystem-accessed storage at monthly to seasonal timescales across many temperate and tropical forests, croplands, and savannas with limited snow cover. At interannual scales, however, the agreement weakens across many ecosystems, as TWSA also carries signals from snow, groundwater, and other storage components that may evolve independently of ecosystem water access. Studies using TWSA as a proxy for ecosystem water availability therefore need to account for the timescale and hydroclimatic regime under which this proxy relationship holds (Khanal et al., 2024).

More broadly, these results show that ecosystem-accessed subsurface storage can be tracked and interpreted as an observation-based dimension of the terrestrial water cycle. Coupling aS_{rz} with carbon flux, phenology, and stress indicators would help clarify how access to subsurface water regulates gross primary production, transpiration efficiency, and drought vulnerability (Choat et al., 2018; Humphrey et al., 2021; Stocker et al., 2019). Comparing aS_{rz} with root-zone soil moisture representations in land surface models offers a path for assessing how models partition water between vegetation use and other subsurface pathways (Giardina et al., 2025). Extending the prognostic reconstruction to longer meteorological forcing records would improve detection of longer-term shifts in ecosystem water access and active storage turnover (Berdugo et al.,

https://doi.org/10.5194/egusphere-2026-3923
Preprint. Discussion started: 20 July 2026

2020; Forzieri et al., 2022). Overall, as hydroclimatic change alters both water supply and demand (McDowell et al., 2022), an observation-based view of the water vegetation actually mobilizes can help identify where ecosystem function is buffered
420 by subsurface storage, where that buffering is becoming compressed in time, and where bulk water cycle indicators provide an incomplete view of ecosystem water change.

Appendix A: Summary of the aS_{rz} reconstruction

The aS_{rz} reconstruction is produced with a differentiable hybrid framework that combines a conceptual ecohydrological model with a neural-network parameterization. The conceptual model represents the subsurface water accessible by
425 ecosystems as a prognostic storage reservoir, while the neural-network parameterization maps static environmental attributes, including climate, vegetation, topography, and soil properties, to spatially varying process parameters. The differentiable structure allows the model to be trained end-to-end against multiple observational constraints, so that ET, runoff, SWE, and TWSA jointly inform learned parameter fields (**Fig. A1**).

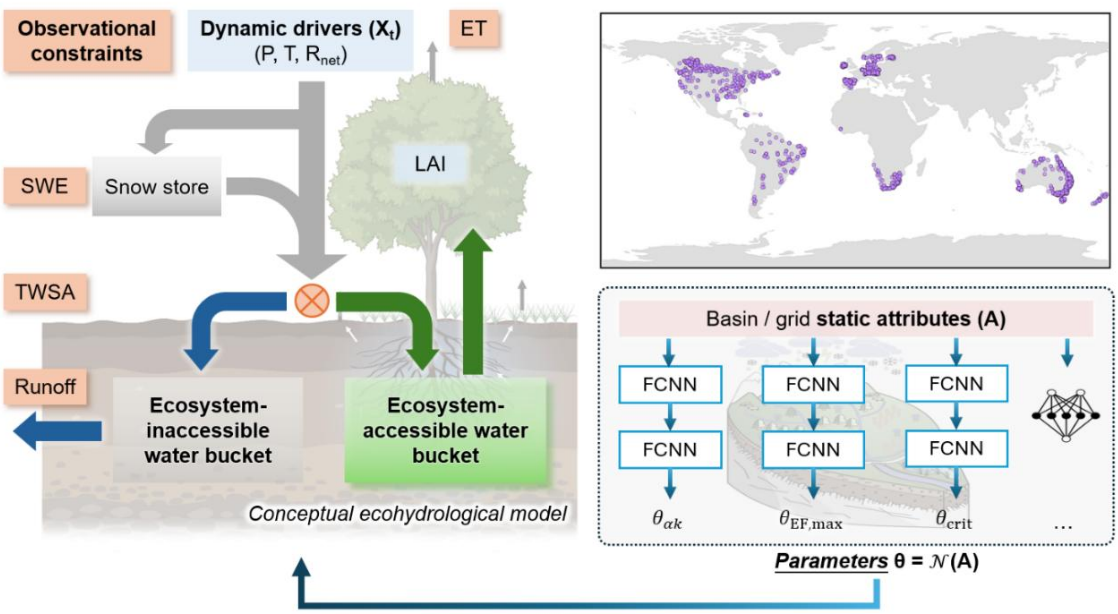

430 **Figure A1. Schematic of the aS_{rz} reconstruction framework.** Dynamic drivers, including precipitation P, air temperature T, net radiation R_{net}, and leaf area index (LAI), force a conceptual ecohydrological model that partitions liquid input into ecosystem-accessible and ecosystem-inaccessible pathways. Liquid input is partitioned between an ecosystem-accessible bucket, which supplies ET, and an ecosystem-inaccessible pathway, which generates runoff through fast and slow stores. ET, runoff, snow water equivalent (SWE), and terrestrial water storage anomalies (TWSA) provide observational constraints

https://doi.org/10.5194/egusphere-2026-3923
Preprint. Discussion started: 20 July 2026

during basin-scale training. The map in the upper right shows the GRDC-Caravan catchments used for training. Static attributes of each basin or grid cell, A, are mapped by fully connected neural networks (FCNNs) to spatially varying process parameters $\theta = \mathcal{N}(A)$. After training, the same parameterization is applied to the global grid to produce the ecosystem-accessible storage S_a, from which aS_rz is diagnosed.

The conceptual core is designed to separate incoming liquid water into an ecosystem-accessible pathway and an ecosystem-inaccessible pathway. Liquid input, consisting of rainfall and snowmelt, is partitioned between these two pathways according to the relative wetness of the ecosystem-accessible storage. The ecosystem-accessible bucket stores water that can be used for ET by ecosystems, while the ecosystem-inaccessible pathway feeds fast and slow runoff stores. At daily time step t, the relative wetness of the accessible storage is defined as $S_\mathrm{moist}^{(t)} = S_\mathrm{a}^{(t)}/\theta_\mathrm{cap} \in [0,1]$, where $S_\mathrm{a}^{(t)}$ is the ecosystem-accessible storage and θ_cap is the storage capacity parameter. The fraction of liquid input routed to the ecosystem-accessible reservoir is $\alpha^{(t)} = \left(1 - S_\mathrm{moist}^{(t-1)}\right)^{\theta_{\alpha k}}$,where $\theta_{\alpha k}$is a learned shape parameter, which follows the logic of nonlinear, moisture-dependent partitioning in conceptual rainfall-runoff models (e.g., Koster and P. Mahanama, 2012; Perrin et al., 2003), where the fraction of incoming water retained in a storage compartment decreases as that compartment fills. The liquid input to the ecosystem-accessible reservoir is therefore $P_\mathrm{eff}^{(t)} = \alpha^{(t)} P_\mathrm{liq}^{(t)}$, and the remaining liquid input, $P_\mathrm{ineff}^{(t)} = (1-\alpha^{(t)}) P_\mathrm{liq}^{(t)}$, is routed to the ecosystem-inaccessible pathway. The ecosystem-accessible storage evolves as $S_\mathrm{a}^{(t)} = S_\mathrm{a}^{(t-1)} + P_\mathrm{eff}^{(t)} - \mathrm{ET}^{(t)}$. ET is computed using a Priestley-Taylor formulation (Priestley and Taylor, 1972), modulated by soil moisture stress and canopy phenology (Koppa et al., 2022). This structure means that S_a is depleted only through ET and therefore represents the subsurface storage functionally accessed by ecosystems. The ecosystem-inaccessible pathway is represented by fast and slow stores following a conceptual runoff-generation structure (Seibert, 1997). The fast store receives P_ineff, generates rapid runoff, and transfers water to the slow store through percolation. The slow store generates delayed baseflow. Total runoff is the sum of fast runoff and slow baseflow, $Q_\mathrm{total}^{(t)} = Q_\mathrm{fast}^{(t)} + Q_\mathrm{slow}^{(t)}$.

The main learned process parameters include the rain-snow partitioning thresholds, the snowmelt factor, the liquid-input partitioning shape parameter $\theta_{\alpha k}$, the ecosystem-accessible storage capacity parameter θ_cap, soil-moisture stress parameters controlling ET reduction, canopy phenology parameters controlling seasonal ET modulation, and fast-flow, percolation, and slow-flow parameters controlling runoff generation. These parameters are predicted from static environmental attributes by the neural-network parameterization and therefore vary across basins and grid cells. The full model description is provided by (Blougouras et al., 2026). The dynamic forcing, static attributes, observational constraints, basin selection, cross-validation design, and global application used to obtain aS_rz are described in **Sect. 2.1**.

https://doi.org/10.5194/egusphere-2026-3923
Preprint. Discussion started: 20 July 2026

Because aS_{rz} is defined from the dynamic range of S_a, it has no direct one-to-one observational counterpart. It therefore cannot be validated in the same way as runoff, snow water equivalent, or near-surface soil moisture. Instead, we assess whether the reconstructed storage states are consistent with independent estimates of root-zone wetness. **Figure A2** compares temporal Pearson correlations between existing gridded root-zone soil moisture products and two reconstructed storage states: the ecosystem-accessible storage S_a, and modeled bulk root-zone storage S_{bulk}, defined as the sum of ecosystem-accessible and ecosystem-inaccessible storages. The comparison uses GLEAM, SoMo.ml, and ERA5-Land root-zone soil moisture, which were not used as training constraints. Because these products differ in units, represented soil depth, and absolute magnitude, the comparison focuses on temporal correlation. As shown in **Fig. A2**, the modeled S_{bulk} is strongly correlated with all three products across most vegetated land areas, indicating that the framework captures broad bulk root-zone wetness dynamics. S_a also covaries with these products in many regions, but correlations are lower in high-latitude, energy-limited, and some dry regions. This divergence is expected because conventional root-zone soil moisture products represent bulk water content within prescribed soil layers, whereas S_a represents the storage component functionally accessed and depleted through ET. The contrast between S_{bulk} and S_a therefore supports the interpretation of S_a as ecosystem-accessible storage. Full model evaluation and benchmarking are provided by (Blougouras et al., 2026).

https://doi.org/10.5194/egusphere-2026-3923
Preprint. Discussion started: 20 July 2026

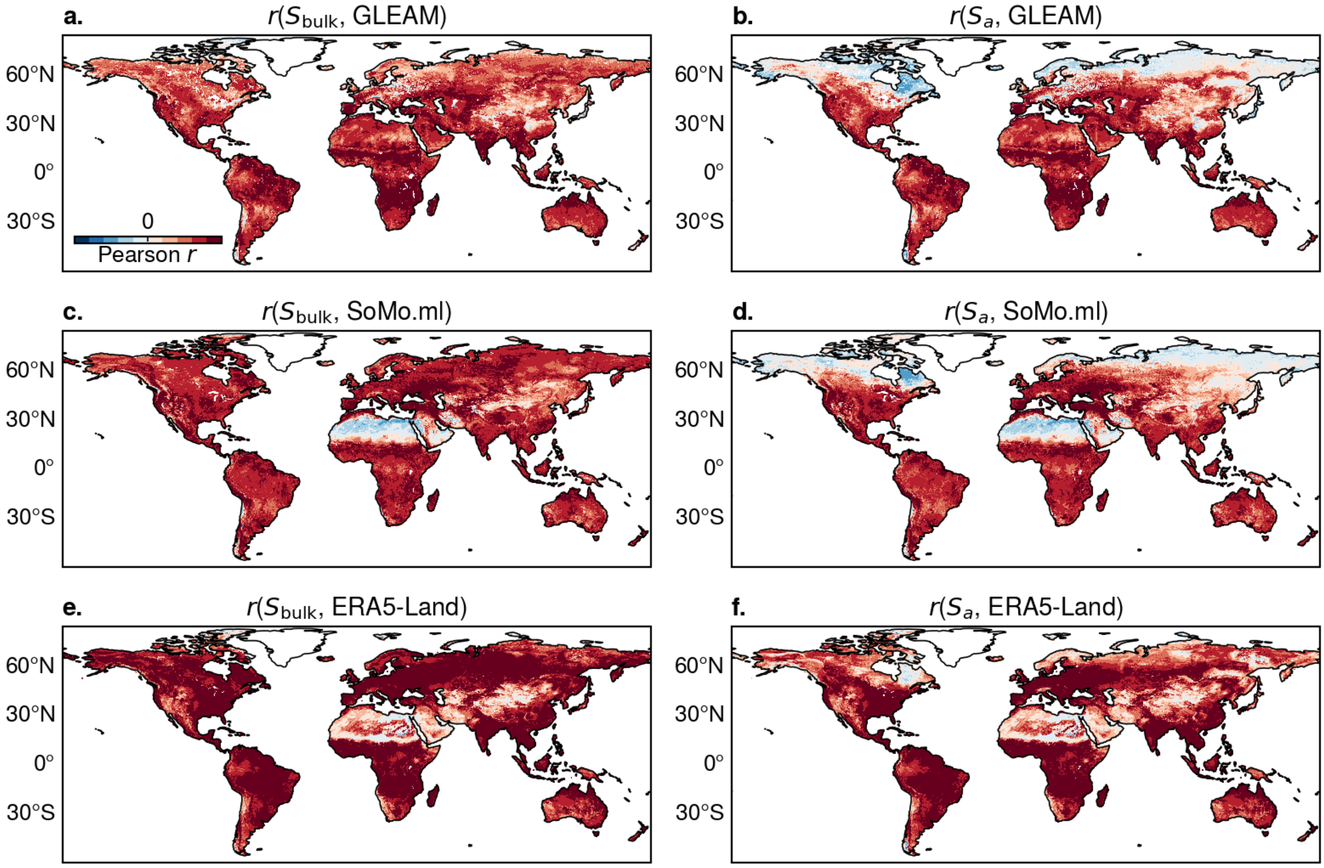

Figure A2. Comparison between reconstructed storage states and global root-zone soil moisture products. Pearson correlations between modelled bulk root-zone storage S_{bulk}, left column, and ecosystem-accessible storage S_{a}, right column, with root-zone soil moisture from GLEAM, panels a and b, SoMo.ml, panels c and d, and ERA5-Land, panels e and f. S_{bulk} is defined as the sum of ecosystem-accessible and ecosystem-inaccessible storages.

Code and data availability

The monthly active root zone water storage fields analyzed in this study are available at https://doi.org/10.5281/zenodo.21136948 (Jiang and Blougouras, 2026). The external datasets used in the analyses are publicly available from their original providers. Terrestrial water storage anomalies used in the coupling analysis were obtained from GRACE and GRACE-FO mascon products (Watkins et al., 2015). Evapotranspiration used to calculate active reservoir turnover time was obtained from FLUXCOM X-BASE (Nelson et al., 2024). Precipitation and meteorological variables used to calculate PET were obtained from ERA5-Land (Muñoz-Sabater et al., 2021). Land cover classes were

https://doi.org/10.5194/egusphere-2026-3923
Preprint. Discussion started: 20 July 2026

derived from the MODIS modified IGBP product (Friedl et al., 2010). Leaf area index was obtained from GIMMS LAI4g (Cao et al., 2023). Terrain slope and snow cover fraction were taken from HydroATLAS (Linke et al., 2019), and soil texture was taken from SoilGrids (Poggio et al., 2021). The reconstruction model code used to produce aS_{rz} is available at https://doi.org/10.5281/zenodo.20692925 (Blougouras and Jiang, 2026).

Author contributions

S.J.: conceptualization, methodology, investigation, formal analysis, data curation, visualization, writing of the original draft, review and editing, supervision, and funding acquisition. G.B.: conceptualization, methodology, investigation, formal analysis, data curation, visualization, writing of the original draft, and review and editing. Both authors approved the final version of the manuscript.

Competing interests

The authors declare that they have no conflict of interest.

Disclaimer

Copernicus Publications remains neutral with regard to jurisdictional claims made in the text, published maps, institutional affiliations, or any other geographical representation in this paper. While Copernicus Publications makes every effort to include appropriate place names, the final responsibility lies with the authors. Views expressed in the text are those of the authors and do not necessarily reflect the views of the publisher.

Acknowledgements

The authors are grateful to Prof. Dr. Markus Reichstein and Dr. Martin Jung for helpful discussions related to this work.

Financial support

This research was supported by the Carl-Zeiss-Stiftung through the Junior Research Group “Knowledge Integration for Spatio-Temporal Environmental Modeling” (P2021-00-008) and the CZS Breakthroughs project GENAI-X (P2024-11-042).

https://doi.org/10.5194/egusphere-2026-3923
Preprint. Discussion started: 20 July 2026

References

Bachofen, C., Tumber-Dávila, S. J., Mackay, D. S., McDowell, N. G., Carminati, A., Klein, T., Stocker, B. D., Mencuccini, M., and Grossiord, C.: Tree water uptake patterns across the globe, New Phytologist, 242, 1891–1910, https://doi.org/10.1111/nph.19762, 2024.

Berdugo, M., Delgado-Baquerizo, M., Soliveres, S., Hernández-Clemente, R., Zhao, Y., Gaitán, J. J., Gross, N., Saiz, H., Maire, V., Lehmann, A., Rillig, M. C., Solé, R. V., and Maestre, F. T.: Global ecosystem thresholds driven by aridity, Science, 367, 787–790, https://doi.org/10.1126/science.aay5958, 2020.

Blougouras, G. and Jiang, S.: MOREDO: A Multi-Observation Root-zone Ecohydrology DiagnOstic model, , https://doi.org/10.5281/zenodo.20692925, 2026.

Blougouras, G., Jiang, S., Brenning, A., Migliavacca, M., Slater, L. J., Zhou, J., Kumar, R., Tian, L., Wang, C., and Reichstein, M.: Spatiotemporal dynamics of active root zone storage revealed from hybrid machine learning, https://doi.org/10.22541/essoar.176280049.93675424/v1, 10 November 2025.

Blougouras, G., Chen, X., Brenning, A., Kumar, R., Migliavacca, M., Reichstein, M., and Jiang, S.: MOREDO: A differentiable hybrid framework for transferable diagnosis of active root-zone water across scales, ESS Open Archive, https://doi.org/10.22541/essoar.15005507/v1, 2026.

Cao, S., Li, M., Zhu, Z., Wang, Z., Zha, J., Zhao, W., Duanmu, Z., Chen, J., Zheng, Y., Chen, Y., Myneni, R. B., and Piao, S.: Spatiotemporally consistent global dataset of the GIMMS leaf area index (GIMMS LAI4g) from 1982 to 2020, Earth Syst. Sci. Data, 15, 4877–4899, https://doi.org/10.5194/essd-15-4877-2023, 2023.

Choat, B., Brodribb, T. J., Brodersen, C. R., Duursma, R. A., López, R., and Medlyn, B. E.: Triggers of tree mortality under drought, Nature, 558, 531–539, https://doi.org/10.1038/s41586-018-0240-x, 2018.

Dorigo, W., Wagner, W., Albergel, C., Albrecht, F., Balsamo, G., Brocca, L., Chung, D., Ertl, M., Forkel, M., Gruber, A., Haas, E., Hamer, P. D., Hirschi, M., Ikonen, J., De Jeu, R., Kidd, R., Lahoz, W., Liu, Y. Y., Miralles, D., Mistelbauer, T., Nicolai-Shaw, N., Parinussa, R., Pratola, C., Reimer, C., Van Der Schalie, R., Seneviratne, S. I., Smolander, T., and Lecomte, P.: ESA CCI soil moisture for improved Earth system understanding: State-of-the art and future directions, Remote Sensing of Environment, 203, 185–215, https://doi.org/10.1016/j.rse.2017.07.001, 2017.

Entekhabi, D., Njoku, E. G., O'Neill, P. E., Kellogg, K. H., Crow, W. T., Edelstein, W. N., Entin, J. K., Goodman, S. D., Jackson, T. J., Johnson, J., Kimball, J., Piepmeier, J. R., Koster, R. D., Martin, N., McDonald, K. C., Moghaddam, M., Moran, S., Reichle, R., Shi, J. C., Spencer, M. W., Thurman, S. W., Tsang, L., and Van Zyl, J.: The Soil Moisture Active Passive (SMAP) mission, Proc. IEEE, 98, 704–716, https://doi.org/10.1109/JPROC.2010.2043918, 2010.

Fan, Y., Miguez-Macho, G., Jobbágy, E. G., Jackson, R. B., and Otero-Casal, C.: Hydrologic regulation of plant rooting depth, Proceedings of the National Academy of Sciences, 114, 10572–10577, https://doi.org/10.1073/pnas.1712381114, 2017.

Fan, Y., Clark, M., Lawrence, D. M., Swenson, S., Band, L. E., Brantley, S. L., Brooks, P. D., Dietrich, W. E., Flores, A., Grant, G., Kirchner, J. W., Mackay, D. S., McDonnell, J. J., Milly, P. C. D., Sullivan, P. L., Tague, C., Ajami, H., Chaney, N., Hartmann, A., Hazenberg, P., McNamara, J., Pelletier, J., Perket, J., Rouholahnejad-Freund, E., Wagener, T., Zeng, X., Beighley, E., Buzan, J., Huang, M., Livneh, B., Mohanty, B. P., Nijssen, B., Safeeq, M., Shen, C., Van Verseveld, W., Volk, J., and Yamazaki, D.: Hillslope Hydrology in Global Change Research and Earth System Modeling, Water Resources Research, 55, 1737–1772, https://doi.org/10.1029/2018WR023903, 2019.

Färber, C., Plessow, H., Mischel, S. A., Kratzert, F., Addor, N., Shalev, G., and Looser, U.: GRDC-Caravan: extending Caravan with data from the Global Runoff Data Centre, Earth Syst. Sci. Data, 17, 4613–4625, https://doi.org/10.5194/essd-17-4613-2025, 2025.

https://doi.org/10.5194/egusphere-2026-3923
Preprint. Discussion started: 20 July 2026

Fatichi, S., Or, D., Walko, R., Vereecken, H., Young, M. H., Ghezzehei, T. A., Hengl, T., Kollet, S., Agam, N., and Avissar, R.: Soil structure is an important omission in Earth System Models, Nature Communications, 11, 522, https://doi.org/10.1038/s41467-020-14411-z, 2020.

Fisher, R. A. and Koven, C. D.: Perspectives on the future of land surface models and the challenges of representing complex terrestrial systems, Journal of Advances in Modeling Earth Systems, 12, e2018MS001453, https://doi.org/10.1029/2018MS001453, 2020.

Forzieri, G., Dakos, V., McDowell, N. G., Ramdane, A., and Cescatti, A.: Emerging signals of declining forest resilience under climate change, Nature, 608, 534–539, https://doi.org/10.1038/s41586-022-04959-9, 2022.

Frappart, F., Ramillien, G., Biancamaria, S., Mognard, N. M., and Cazenave, A.: Evolution of high-latitude snow mass derived from the GRACE gravimetry mission (2002–2004), Geophysical Research Letters, 33, 2005GL024778, https://doi.org/10.1029/2005GL024778, 2006.

Friedl, M. A., Sulla-Menashe, D., Tan, B., Schneider, A., Ramankutty, N., Sibley, A., and Huang, X.: MODIS Collection 5 global land cover: Algorithm refinements and characterization of new datasets, Remote Sensing of Environment, 114, 168–182, https://doi.org/10.1016/j.rse.2009.08.016, 2010.

Gao, H., Hrachowitz, M., Schymanski, S. J., Fenicia, F., Sriwongsitanon, N., and Savenije, H. H. G.: Climate controls how ecosystems size the root zone storage capacity at catchment scale, Geophysical Research Letters, 41, 7916–7923, https://doi.org/10.1002/2014GL061668, 2014.

Gao, H., Hrachowitz, M., Wang-Erlandsson, L., Fenicia, F., Xi, Q., Xia, J., Shao, W., Sun, G., and Savenije, H. H. G.: Root zone in the Earth system, Hydrol. Earth Syst. Sci., 28, 4477–4499, https://doi.org/10.5194/hess-28-4477-2024, 2024.

Gentine, P., Green, J. K., Guérin, M., Humphrey, V., Seneviratne, S. I., Zhang, Y., and Zhou, S.: Coupling between the terrestrial carbon and water cycles—a review, Environ. Res. Lett., 14, 083003, https://doi.org/10.1088/1748-9326/ab22d6, 2019.

Giardina, F., Padrón, R. S., Stocker, B. D., Schumacher, D. L., and Seneviratne, S. I.: Large biases in the frequency of water limitation across Earth system models, Commun Earth Environ, 6, 469, https://doi.org/10.1038/s43247-025-02426-7, 2025.

Gnann, S., Baldwin, J. W., Cuthbert, M. O., Gleeson, T., Schwanghart, W., and Wagener, T.: The influence of topography on the global terrestrial water cycle, Reviews of Geophysics, 63, e2023RG000810, https://doi.org/10.1029/2023RG000810, 2025.

Goulden, M. L. and Bales, R. C.: California forest die-off linked to multi-year deep soil drying in 2012–2015 drought, Nat. Geosci., 12, 632–637, https://doi.org/10.1038/s41561-019-0388-5, 2019.

Green, J. K., Seneviratne, S. I., Berg, A. M., Findell, K. L., Hagemann, S., Lawrence, D. M., and Gentine, P.: Large influence of soil moisture on long-term terrestrial carbon uptake, Nature, 565, 476–479, https://doi.org/10.1038/s41586-018-0848-x, 2019.

Humphrey, V., Zscheischler, J., Ciais, P., Gudmundsson, L., Sitch, S., and Seneviratne, S. I.: Sensitivity of atmospheric CO2 growth rate to observed changes in terrestrial water storage, Nature, 560, 628–631, https://doi.org/10.1038/s41586-018-0424-4, 2018.

Humphrey, V., Berg, A., Ciais, P., Gentine, P., Jung, M., Reichstein, M., Seneviratne, S. I., and Frankenberg, C.: Soil moisture–atmosphere feedback dominates land carbon uptake variability, Nature, 592, 65–69, https://doi.org/10.1038/s41586-021-03325-5, 2021.

Humphrey, V., Rodell, M., and Eicker, A.: Using Satellite-Based Terrestrial Water Storage Data: A Review, Surv Geophys, 44, 1489–1517, https://doi.org/10.1007/s10712-022-09754-9, 2023.

Jiang, S. and Blougouras, G.: Global active root-zone water storage, https://doi.org/10.5281/zenodo.21136948, 2026.

Jung, M., Schwalm, C., Migliavacca, M., Walther, S., Camps-Valls, G., Koirala, S., Anthoni, P., Besnard, S., Bodesheim, P., Carvalhais, N., Chevallier, F., Gans, F., Goll, D. S., Haverd, V., Köhler, P., Ichii, K., Jain, A. K., Liu, J., Lombardozzi, D., Nabel, J. E. M. S., Nelson, J. A., O'Sullivan, M., Pallandt, M., Papale, D., Peters, W., Pongratz, J., Rödenbeck, C., Sitch, S., Tramontana, G., Walker, A., Weber, U., and Reichstein, M.: Scaling carbon fluxes from eddy covariance sites to globe: synthesis and evaluation of the FLUXCOM approach, Biogeosciences, 17, 1343–1365, https://doi.org/10.5194/bg-17-1343-2020, 2020.

Khanal, P., Hoek Van Dijke, A. J., Schaffhauser, T., Li, W., Paulus, S. J., Zhan, C., and Orth, R.: Relevance of near-surface soil moisture vs. terrestrial water storage for global vegetation functioning, Biogeosciences, 21, 1533–1547, https://doi.org/10.5194/bg-21-1533-2024, 2024.

Knapp, A. K., Beier, C., Briske, D. D., Classen, A. T., Luo, Y., Reichstein, M., Smith, M. D., Smith, S. D., Bell, J. E., Fay, P. A., Heisler, J. L., Leavitt, S. W., Sherry, R., Smith, B., and Weng, E.: Consequences of More Extreme Precipitation Regimes for Terrestrial Ecosystems, BioScience, 58, 811–821, https://doi.org/10.1641/B580908, 2008.

Koppa, A., Rains, D., Hulsman, P., Poyatos, R., and Miralles, D. G.: A deep learning-based hybrid model of global terrestrial evaporation, Nat Commun, 13, 1912, https://doi.org/10.1038/s41467-022-29543-7, 2022.

Koster, R. D. and P. Mahanama, S. P.: Land Surface Controls on Hydroclimatic Means and Variability, Journal of Hydrometeorology, 13, 1604–1620, https://doi.org/10.1175/JHM-D-12-050.1, 2012.

Krabbenhoft, C. A., Allen, G. H., Lin, P., Godsey, S. E., Allen, D. C., Burrows, R. M., DelVecchia, A. G., Fritz, K. M., Shanafield, M., Burgin, A. J., Zimmer, M. A., Datry, T., Dodds, W. K., Jones, C. N., Mims, M. C., Franklin, C., Hammond, J. C., Zipper, S., Ward, A. S., Costigan, K. H., Beck, H. E., and Olden, J. D.: Assessing placement bias of the global river gauge network, Nat Sustain, 5, 586–592, https://doi.org/10.1038/s41893-022-00873-0, 2022.

Landerer, F. W., Flechtner, F. M., Save, H., Webb, F. H., Bandikova, T., Bertiger, W. I., Bettadpur, S. V., Byun, S. H., Dahle, C., Dobslaw, H., Fahnestock, E., Harvey, N., Kang, Z., Kruizinga, G. L. H., Loomis, B. D., McCullough, C., Murböck, M., Nagel, P., Paik, M., Pie, N., Poole, S., Strekalov, D., Tamisiea, M. E., Wang, F., Watkins, M. M., Wen, H., Wiese, D. N., and Yuan, D.: Extending the global mass change data record: GRACE Follow-On instrument and science data performance, Geophysical Research Letters, 47, e2020GL088306, https://doi.org/10.1029/2020GL088306, 2020.

Lesk, C., Rowhani, P., and Ramankutty, N.: Influence of extreme weather disasters on global crop production, Nature, 529, 84–87, https://doi.org/10.1038/nature16467, 2016.

Lesk, C. S. and Mankin, J. S.: More concentrated precipitation decreases terrestrial water storage, Nature, 653, 425–432, https://doi.org/10.1038/s41586-026-10487-7, 2026.

Linke, S., Lehner, B., Ouellet Dallaire, C., Ariwi, J., Grill, G., Anand, M., Beames, P., Burchard-Levine, V., Maxwell, S., Moidu, H., Tan, F., and Thieme, M.: Global hydro-environmental sub-basin and river reach characteristics at high spatial resolution, Sci Data, 6, 283, https://doi.org/10.1038/s41597-019-0300-6, 2019.

Lu, J., Kong, D., Zhang, Y., Xie, Y., Gu, X., and Gulakhmadov, A.: Hotspots of Global Water Resource Changes and Their Causes, Earth's Future, 13, e2024EF005461, https://doi.org/10.1029/2024EF005461, 2025.

Maxwell, R. M. and Condon, L. E.: Connections between groundwater flow and transpiration partitioning, Science, 353, 377–380, https://doi.org/10.1126/science.aaf7891, 2016.

McCormick, E. L., Dralle, D. N., Hahm, W. J., Tune, A. K., Schmidt, L. M., Chadwick, K. D., and Rempe, D. M.: Widespread woody plant use of water stored in bedrock, Nature, 597, 225–229, https://doi.org/10.1038/s41586-021-03761-3, 2021.

McDowell, N. G., Sapes, G., Pivovaroff, A., Adams, H. D., Allen, C. D., Anderegg, W. R. L., Arend, M., Breshears, D. D., Brodribb, T., Choat, B., Cochard, H., De Cáceres, M., De Kauwe, M. G., Grossiord, C., Hammond, W. M., Hartmann, H., Hoch, G., Kahmen, A., Klein, T., Mackay, D. S., Mantova, M., Martínez-Vilalta, J., Medlyn, B. E., Mencuccini, M., Nardini, A., Oliveira, R. S., Sala, A., Tissue, D. T., Torres-Ruiz, J. M., Trowbridge, A. M., Trugman, A. T., Wiley, E., and Xu, C.: Mechanisms of woody-plant mortality under rising drought, CO2 and vapour pressure deficit, Nat Rev Earth Environ, 3, 294–308, https://doi.org/10.1038/s43017-022-00272-1, 2022.

Miguez-Macho, G. and Fan, Y.: The role of groundwater in the Amazon water cycle: 2. Influence on seasonal soil moisture and evapotranspiration, J. Geophys. Res., 117, 2012JD017540, https://doi.org/10.1029/2012JD017540, 2012.

Miralles, D. G., Gentine, P., Seneviratne, S. I., and Teuling, A. J.: Land–atmospheric feedbacks during droughts and heatwaves: state of the science and current challenges, Annals of the New York Academy of Sciences, 1436, 19–35, https://doi.org/10.1111/nyas.13912, 2019.

Muñoz-Sabater, J., Dutra, E., Agustí-Panareda, A., Albergel, C., Arduini, G., Balsamo, G., Boussetta, S., Choulga, M., Harrigan, S., Hersbach, H., Martens, B., Miralles, D. G., Piles, M., Rodríguez-Fernández, N. J., Zsoter, E., Buontempo, C., and Thépaut, J.-N.: ERA5-Land: A state-of-the-art global reanalysis dataset for land applications, Earth Syst. Sci. Data, 13, 4349–4383, https://doi.org/10.5194/essd-13-4349-2021, 2021.

Myers-Smith, I. H., Kerby, J. T., Phoenix, G. K., Bjerke, J. W., Epstein, H. E., Assmann, J. J., John, C., Andreu-Hayles, L., Angers-Blondin, S., Beck, P. S. A., Berner, L. T., Bhatt, U. S., Bjorkman, A. D., Blok, D., Bryn, A., Christiansen, C. T., Cornelissen, J. H. C., Cunliffe, A. M., Elmendorf, S. C., Forbes, B. C., Goetz, S. J., Hollister, R. D., De Jong, R., Loranty, M. M., Macias-Fauria, M., Maseyk, K., Normand, S., Olofsson, J., Parker, T. C., Parmentier, F.-J. W., Post, E., Schaepman-Strub, G., Stordal, F., Sullivan, P. F., Thomas, H. J. D., Tømmervik, H., Treharne, R., Tweedie, C. E., Walker, D. A., Wilmking, M., and Wipf, S.: Complexity revealed in the greening of the Arctic, Nat. Clim. Chang., 10, 106–117, https://doi.org/10.1038/s41558-019-0688-1, 2020.

Nadolski, L., Wesselkamp, M., El-Madany, T., Lange, M., Nelson, J., Carrara, A., Wieckowski, A., Hildebrandt, A., Reichstein, M., and Lee, S.-C.: Impacts of Precipitation Variability on Carbon Flux Dynamics of Global Semi-Arid Savannas, Global Change Biology, 32, e70954, https://doi.org/10.1111/gcb.70954, 2026.

Nelson, J. A., Walther, S., Gans, F., Kraft, B., Weber, U., Novick, K., Buchmann, N., Migliavacca, M., Wohlfahrt, G., Šigut, L., Ibrom, A., Papale, D., Göckede, M., Duveiller, G., Knohl, A., Hörtnagl, L., Scott, R. L., Dušek, J., Zhang, W., Hamdi, Z. M., Reichstein, M., Aranda-Barranco, S., Ardö, J., Op De Beeck, M., Billesbach, D., Bowling, D., Bracho, R., Brümmer, C., Camps-Valls, G., Chen, S., Cleverly, J. R., Desai, A., Dong, G., El-Madany, T. S., Euskirchen, E. S., Feigenwinter, I., Galvagno, M., Gerosa, G. A., Gielen, B., Goded, I., Goslee, S., Gough, C. M., Heinesch, B., Ichii, K., Jackowicz-Korczynski, M. A., Klosterhalfen, A., Knox, S., Kobayashi, H., Kohonen, K.-M., Korkiakoski, M., Mammarella, I., Gharun, M., Marzuoli, R., Matamala, R., Metzger, S., Montagnani, L., Nicolini, G., O'Halloran, T., Ourcival, J.-M., Peichl, M., Pendall, E., Ruiz Reverter, B., Roland, M., Sabbatini, S., Sachs, T., Schmidt, M., Schwalm, C. R., Shekhar, A., Silberstein, R., Silveira, M. L., Spano, D., Tagesson, T., Tramontana, G., Trotta, C., Turco, F., Vesala, T., Vincke, C., Vitale, D., Vivoni, E. R., Wang, Y., Woodgate, W., Yepez, E. A., Zhang, J., Zona, D., and Jung, M.: X-BASE: The first terrestrial carbon and water flux products from an extended data-driven scaling framework, FLUXCOM-X, Biogeosciences, 21, 5079–5115, https://doi.org/10.5194/bg-21-5079-2024, 2024.

Neumann, R. B. and Cardon, Z. G.: The magnitude of hydraulic redistribution by plant roots: a review and synthesis of empirical and modeling studies, New Phytologist, 194, 337–352, https://doi.org/10.1111/j.1469-8137.2012.04088.x, 2012.

Noormets, A., McNulty, S. G., DeForest, J. L., Sun, G., Li, Q., and Chen, J.: Drought during canopy development has lasting effect on annual carbon balance in a deciduous temperate forest, New Phytologist, 179, 818–828, https://doi.org/10.1111/j.1469-8137.2008.02501.x, 2008.

Perrin, C., Michel, C., and Andréassian, V.: Improvement of a parsimonious model for streamflow simulation, Journal of Hydrology, 279, 275–289, https://doi.org/10.1016/S0022-1694(03)00225-7, 2003.

Phillips, T., Nerem, R. S., Fox-Kemper, B., Famiglietti, J. S., and Rajagopalan, B.: The influence of ENSO on global terrestrial water storage using GRACE, Geophysical Research Letters, 39, 2012GL052495, https://doi.org/10.1029/2012GL052495, 2012.

Poggio, L., De Sousa, L. M., Batjes, N. H., Heuvelink, G. B. M., Kempen, B., Ribeiro, E., and Rossiter, D.: SoilGrids 2.0: producing soil information for the globe with quantified spatial uncertainty, SOIL, 7, 217–240, https://doi.org/10.5194/soil-7-217-2021, 2021.

Priestley, C. H. B. and Taylor, R. J.: On the Assessment of Surface Heat Flux and Evaporation Using Large-Scale Parameters, Mon. Wea. Rev., 100, 81–92, https://doi.org/10.1175/1520-0493(1972)100%3C0081:OTAOSH%3E2.3.CO;2, 1972.

Qing, Y., Wang, S., Yang, Z.-L., Gentine, P., Zhang, B., and Alexander, J.: Accelerated soil drying linked to increasing evaporative demand in wet regions, npj Clim Atmos Sci, 6, 205, https://doi.org/10.1038/s41612-023-00531-y, 2023.

Reichle, R. H., Liu, Q., Koster, R. D., Crow, W. T., De Lannoy, G. J. M., Kimball, J. S., Ardizzone, J. V., Bosch, D., Colliander, A., Cosh, M., Kolassa, J., Mahanama, S. P., Prueger, J., Starks, P., and Walker, J. P.: Version 4 of the SMAP Level-4 soil moisture algorithm and data product, J Adv Model Earth Syst, 11, 3106–3130, https://doi.org/10.1029/2019MS001729, 2019.

Reichstein, M., Bahn, M., Ciais, P., Frank, D., Mahecha, M. D., Seneviratne, S. I., Zscheischler, J., Beer, C., Buchmann, N., Frank, D. C., Papale, D., Rammig, A., Smith, P., Thonicke, K., Van Der Velde, M., Vicca, S., Walz, A., and Wattenbach, M.: Climate extremes and the carbon cycle, Nature, 500, 287–295, https://doi.org/10.1038/nature12350, 2013.

Rempe, D. M. and Dietrich, W. E.: Direct observations of rock moisture, a hidden component of the hydrologic cycle, Proc. Natl. Acad. Sci. U.S.A., 115, 2664–2669, https://doi.org/10.1073/pnas.1800141115, 2018.

Restrepo-Coupe, N., Da Rocha, H. R., Hutyra, L. R., Da Araujo, A. C., Borma, L. S., Christoffersen, B., Cabral, O. M. R., De Camargo, P. B., Cardoso, F. L., Da Costa, A. C. L., Fitzjarrald, D. R., Goulden, M. L., Kruijt, B., Maia, J. M. F., Malhi, Y. S., Manzi, A. O., Miller, S. D., Nobre, A. D., Von Randow, C., Sá, L. D. A., Sakai, R. K., Tota, J., Wofsy, S. C., Zanchi, F. B., and Saleska, S. R.: What drives the seasonality of photosynthesis across the Amazon basin? A cross-site analysis of eddy flux tower measurements from the Brasil flux network, Agricultural and Forest Meteorology, 182–183, 128–144, https://doi.org/10.1016/j.agrformet.2013.04.031, 2013.

Rodell, M., Famiglietti, J. S., Wiese, D. N., Reager, J. T., Beaudoing, H. K., Landerer, F. W., and Lo, M.-H.: Emerging trends in global freshwater availability, Nature, 557, 651–659, https://doi.org/10.1038/s41586-018-0123-1, 2018.

Saatchi, S., Asefi-Najafabady, S., Malhi, Y., Aragão, L. E. O. C., Anderson, L. O., Myneni, R. B., and Nemani, R.: Persistent effects of a severe drought on Amazonian forest canopy, Proc. Natl. Acad. Sci. U.S.A., 110, 565–570, https://doi.org/10.1073/pnas.1204651110, 2013.

Scanlon, B. R., Zhang, Z., Save, H., Sun, A. Y., Müller Schmied, H., Van Beek, L. P. H., Wiese, D. N., Wada, Y., Long, D., Reedy, R. C., Longuevergne, L., Döll, P., and Bierkens, M. F. P.: Global models underestimate large decadal declining and rising water storage trends relative to GRACE satellite data, Proc. Natl. Acad. Sci. U.S.A., 115, https://doi.org/10.1073/pnas.1704665115, 2018.

Schenk, H. J. and Jackson, R. B.: The global biogeography of roots, Ecological Monographs, 72, 311–328, https://doi.org/10.1890/0012-9615(2002)072%5B0311:TGBOR%5D2.0.CO;2, 2002.

Schimel, D., Pavlick, R., Fisher, J. B., Asner, G. P., Saatchi, S., Townsend, P., Miller, C., Frankenberg, C., Hibbard, K., and Cox, P.: Observing terrestrial ecosystems and the carbon cycle from space, Global Change Biology, 21, 1762–1776, https://doi.org/10.1111/gcb.12822, 2015.

Schuldt, B., Buras, A., Arend, M., Vitasse, Y., Beierkuhnlein, C., Damm, A., Gharun, M., Grams, T. E. E., Hauck, M., Hajek, P., Hartmann, H., Hiltbrunner, E., Hoch, G., Holloway-Phillips, M., Körner, C., Larysch, E., Lübbe, T., Nelson,

D. B., Rammig, A., Rigling, A., Rose, L., Ruehr, N. K., Schumann, K., Weiser, F., Werner, C., Wohlgemuth, T., Zang, C. S., and Kahmen, A.: A first assessment of the impact of the extreme 2018 summer drought on Central European forests, Basic and Applied Ecology, 45, 86–103, https://doi.org/10.1016/j.baae.2020.04.003, 2020.

Schwalm, C. R., Anderegg, W. R. L., Michalak, A. M., Fisher, J. B., Biondi, F., Koch, G., Litvak, M., Ogle, K., Shaw, J. D., Wolf, A., Huntzinger, D. N., Schaefer, K., Cook, R., Wei, Y., Fang, Y., Hayes, D., Huang, M., Jain, A., and Tian, H.: Global patterns of drought recovery, Nature, 548, 202–205, https://doi.org/10.1038/nature23021, 2017.

Seibert, J.: Estimation of Parameter Uncertainty in the HBV Model, Hydrology Research, 28, 247–262, https://doi.org/10.2166/nh.1998.15, 1997.

Seneviratne, S. I., Corti, T., Davin, E. L., Hirschi, M., Jaeger, E. B., Lehner, I., Orlowsky, B., and Teuling, A. J.: Investigating soil moisture–climate interactions in a changing climate: A review, Earth-Science Reviews, 99, 125–161, https://doi.org/10.1016/j.earscirev.2010.02.004, 2010.

Sprenger, M., Stumpp, C., Weiler, M., Aeschbach, W., Allen, S. T., Benettin, P., Dubbert, M., Hartmann, A., Hrachowitz, M., Kirchner, J. W., McDonnell, J. J., Orlowski, N., Penna, D., Pfahl, S., Rinderer, M., Rodriguez, N., Schmidt, M., and Werner, C.: The Demographics of Water: A Review of Water Ages in the Critical Zone, Reviews of Geophysics, 57, 800–834, https://doi.org/10.1029/2018RG000633, 2019.

Stocker, B. D., Zscheischler, J., Keenan, T. F., Prentice, I. C., Seneviratne, S. I., and Peñuelas, J.: Drought impacts on terrestrial primary production underestimated by satellite monitoring, Nat. Geosci., 12, 264–270, https://doi.org/10.1038/s41561-019-0318-6, 2019.

Stocker, B. D., Tumber-Dávila, S. J., Konings, A. G., Anderson, M. C., Hain, C., and Jackson, R. B.: Global patterns of water storage in the rooting zones of vegetation, Nat. Geosci., 16, 250–256, https://doi.org/10.1038/s41561-023-01125-2, 2023.

Vicente-Serrano, S. M., Gouveia, C., Camarero, J. J., Beguería, S., Trigo, R., López-Moreno, J. I., Azorín-Molina, C., Pasho, E., Lorenzo-Lacruz, J., Revuelto, J., Morán-Tejeda, E., and Sanchez-Lorenzo, A.: Response of vegetation to drought time-scales across global land biomes, Proc. Natl. Acad. Sci. U.S.A., 110, 52–57, https://doi.org/10.1073/pnas.1207068110, 2013.

Wang-Erlandsson, L., Bastiaanssen, W. G. M., Gao, H., Jägermeyr, J., Senay, G. B., van Dijk, A. I. J. M., Guerschman, J. P., Keys, P. W., Gordon, L. J., and Savenije, H. H. G.: Global root zone storage capacity from satellite-based evaporation, Hydrol. Earth Syst. Sci., 20, 1459–1481, https://doi.org/10.5194/hess-20-1459-2016, 2016.

Wankmüller, F. J. P., Delval, L., Lehmann, P., Baur, M. J., Cecere, A., Wolf, S., Or, D., Javaux, M., and Carminati, A.: Global influence of soil texture on ecosystem water limitation, Nature, 635, 631–638, https://doi.org/10.1038/s41586-024-08089-2, 2024.

Warren, J. M., Hanson, P. J., Iversen, C. M., Kumar, J., Walker, A. P., and Wullschleger, S. D.: Root structural and functional dynamics in terrestrial biosphere models – evaluation and recommendations, New Phytologist, 205, 59–78, https://doi.org/10.1111/nph.13034, 2015.

Watkins, M. M., Wiese, D. N., Yuan, D., Boening, C., and Landerer, F. W.: Improved methods for observing Earth's time variable mass distribution with GRACE using spherical cap mascons, JGR Solid Earth, 120, 2648–2671, https://doi.org/10.1002/2014JB011547, 2015.

Werth, S., White, D., and Bliss, D. W.: GRACE Detected Rise of Groundwater in the Sahelian Niger River Basin, JGR Solid Earth, 122, https://doi.org/10.1002/2017JB014845, 2017.

Yang, C., Condon, L. E., and Maxwell, R. M.: Unravelling groundwater–stream connections over the continental United States, Nat Water, 3, 70–79, https://doi.org/10.1038/s44221-024-00366-8, 2025.